CDDpress

www.nature.com/cdd

ARTICLE

Check for updates

Ezh2 competes with p53 to license lncRNA *Neat1* transcription for inflammasome activation

Jia Yuan[1,2,5], Qingchen Zhu[2,5], Xingli Zhang[2], Zhenzhen Wen[1], Guiheng Zhang[2], Ni Li[2], Yifei Pei[2], Yan Wang[2], Siyu Pei[2,3], Jing Xu[2], Pan Jia[2], Chao Peng[4], Wei Lu[2], Jun Qin[2], Qian Cao[1]✉ and Yichuan Xiao[2]✉

Inflammasome contributes to the pathogenesis of various inflammatory diseases, but the epigenetic mechanism controlling its activation remains elusive. Here, we found that the histone methyltransferase Ezh2 mediates the activation of multiple types of inflammasomes in macrophages/microglia independent of its methyltransferase activity and thus promotes inflammasome-related pathologies. Mechanistically, Ezh2 functions through its SANT2 domain to maintain the enrichment of H3K27 acetylation in the promoter region of the long noncoding RNA (lncRNA) *Neat1*, thereby promoting chromatin accessibility and facilitating p65-mediated transcription of *Neat1*, which is a critical mediator of inflammasome assembly and activation. In addition, the tumour suppressor protein p53 competes with Ezh2 for the same binding region in the *Neat1* promoter and thus antagonises Ezh2-induced *Neat1* transcription and inflammasome activation. Therefore, loss of Ezh2 strongly promotes the binding of p53, which recruits the deacetylase SIRT1 for H3K27 deacetylation of the *Neat1* promoter and thus suppresses *Neat1* transcription and inflammasome activation. Overall, our study demonstrates an epigenetic mechanism involved in modulating inflammasome activation through an Ezh2/p53 competition model and highlights a novel function of Ezh2 in maintaining H3K27 acetylation to support lncRNA *Neat1* transcription.

Cell Death & Differentiation (2022) 29:2009–2023; https://doi.org/10.1038/s41418-022-00992-3

INTRODUCTION

Inflammasomes are a group of cytosolic protein complexes found mainly in innate immune cells that are widely involved in ageing-related inflammaging, neurodegeneration and other inflammatory diseases, such as inflammatory bowel disease (IBD), Parkinson's disease (PD) and gouty arthritis (GA) [1–3]. The activation of inflammasomes requires a two-step process comprising priming and assembly phases. The priming phase involves the activation of nuclear factor κB and subsequent transcriptional induction of inflammasome components, including Nucleotide-binding domain, leucine-rich-repeat-containing receptors (NLRs), absent in melanoma 2 (AIM2) and pro-interleukin (IL)−1β/IL-18 [4]. The assembly phase is initiated by NLR proteins to sense different exogenous or endogenous stimuli or danger signals, such as adenosine triphosphate (ATP), K^+ efflux, and microbial components, leading to the formation of multiprotein complexes and activation of the inflammasome [5]. The multiprotein complex of the inflammasome consists of different types of sensor proteins, the common adaptor protein apoptosis-associated speck-like protein containing a caspase recruitment domain (ASC) and the effector protein pro-caspase-1, which finally facilitates caspase-1 activation and subsequent maturation and secretion of IL-1β and IL-18 [4]. The ASC protein is the shared adaptor for the assembly and activation of almost all types of inflammasomes, and its oligomerization represents an important early molecular event for the activation of these inflammasomes [6]. Published reports have demonstrated that phosphorylation or linear ubiquitination of ASC is required for its oligomerization [7]. A recent study suggested that the long noncoding RNA (lncRNA) *Neat1* promotes ASC oligomerization, leading to enhanced activation of multiple types of inflammasomes [8]. Despite this research progress, the mechanism controlling ASC oligomerization and subsequent inflammasome activation is still poorly understood.

Ezh2, the catalytic subunit of polycomb repressive complex 2 (PRC2), is mainly involved in repressing gene expression by mediating histone H3K27 trimethylation (H3K27me3), and its biological function is largely dependent on its SET domain-mediated methyltransferase activity [9, 10]. To date, published studies have shown that Ezh2 is highly expressed in cancerous tissues, including prostate and breast cancer tissues [11–13]. Therefore, Ezh2 functions as a potential therapeutic target for cancer, and its most potent inhibitor, GSK126, which inhibits Ezh2-mediated H3K27me3 without affecting the protein level of Ezh2, has been applied in clinical trials for the treatment of several types of cancer [14]. Remarkably, Ezh2 also plays an important role in regulating immune cell functions, especially in innate immune

[1]Department of Gastroenterology, Sir Run Run Shaw Hospital, College of Medicine Zhejiang University, Hangzhou 310016, China. [2]CAS Key Laboratory of Tissue Microenvironment and Tumor, Shanghai Institute of Nutrition and Health, University of Chinese Academy of Sciences, Chinese Academy of Sciences, Shanghai 200031, China. [3]Department of Thoracic Surgical Oncology, Shanghai Lung Cancer Center, Shanghai Chest Hospital, Shanghai Jiao Tong University School of Medicine, Shanghai, China. [4]National Facility for Protein Science in Shanghai, Zhangjiang Lab, Shanghai 201210, China. [5]These authors contributed equally: Jia Yuan, Qingchen Zhu. ✉email: caoq@zju.edu.cn; ycxiao@sibs.ac.cn

Edited by A. Degterev

Received: 1 November 2021 Revised: 18 March 2022 Accepted: 22 March 2022
Published online: 14 May 2022

cells. We previously demonstrated that Ezh2 functions as a histone methyltransferase to promote pro-inflammatory macrophage/microglia activation through H3K27me3-mediated transcriptional inhibition of the anti-inflammatory factor SOCS3 [15]. In dendritic cells, Ezh2 controls cell adhesion and migration through direct methylation of the extranuclear regulatory protein Talin [16]. These findings suggest that Ezh2 may be a potential candidate molecular target for suppressing innate immune activation and related inflammatory diseases. However, whether and how Ezh2-mediated epigenetic modulation affects inflammasome activation is not clear.

RESULTS

Ezh2 enhances inflammasome activation

Clinical data from a public dataset showed that *EZH2* expression was significantly enhanced in the peripheral blood or tissues of patients with various autoimmune diseases and neurodegenerative diseases compared to healthy controls (Fig. S1). Since inflammasomes are widely involved in these diseases, we investigated the potential functions of Ezh2 in inflammasome activation by using mice with myeloid cell *Ezh2* conditional knockout (hereafter called *Ezh2-MKO*) and their littermate wild-type (WT) control mice [15]. *Ezh2* deficiency had no effects on the mRNA expression of lipopolysaccharide (LPS)-induced *Il1b*, *Asc*, *Caspase-1* (*Casp1*) and *Nlrp3* and their protein levels in peritoneal macrophages (Fig. S2A, B), suggesting that Ezh2 is dispensable for the priming step of inflammasome activation. However, *Ezh2* deletion greatly inhibited IL-1β secretion in LPS-primed peritoneal macrophages stimulated by ATP, nigericin, poly(dA:dT) and flagellin (Fig. 1A), suggesting that Ezh2 functions in the assembly phase to ubiquitously activate the NLRP3, AIM2 and NLRC4 inflammasomes. Caspase-1 cleavage is essential for the maturation and release of IL-1β after inflammasome assembly [17]. Accordingly, the processing of pro-caspase-1 p45 to p20 was significantly reduced in LPS-primed *Ezh2*-deficient macrophages stimulated with nigericin, poly(dA:dT) or flagellin (Fig. 1, B-D). In addition, caspase-1-mediated cleavage of gasdermin D (GSDMD) was also impaired in *Ezh2*-deficient macrophages (Fig. S2C).

To further assess the role of Ezh2 in modulating inflammasomes in vivo, we intraperitoneally injected MSU, a commonly used NLRP3 inflammasome stimulator, or thioglycolate broth (TB) into WT and *Ezh2-MKO* mice. As expected, the IL-1β level in lavage fluid was lower and the number of peritoneal exudate cells (PECs) was lower in MSU-treated *Ezh2-MKO* mice than in WT mice. However, this phenotype was not observed in TB-treated WT and *Ezh2-MKO* mice (Fig. 1E–G). Similarly, *Ezh2* deficiency also decreased IL-1β production and PEC numbers in the lavage fluid after challenge with alum, which is also a specific NLRP3 inflammasome inducer (Fig. S2D, E) [18]. In addition, IL-1β blocking antibody decreased IL-1β production and the PEC numbers in the lavage fluid with no significant difference between WT and *Ezh2*-MKO mice that were treated with MSU (Fig. 1E, F), which further confirmed that Ezh2 specifically mediated inflammasome activation in vivo.

To assess the ubiquitous effect of Ezh2 in modulating inflammasome activation, we cultured primary microglia from newborn WT and *Ezh2-MKO* mice. Consistent with the data obtained from peritoneal macrophages, *Ezh2* deficiency also greatly impaired NLRP3 and AIM2 inflammasome activation in microglia, as reflected by decreased IL-1β secretion and Caspase-1 cleavage in *Ezh2*-KO microglia stimulated with nigericin or poly(dA:dT) (Fig. 2A–C). Microglial NLRP3 inflammasome activation is known to mediate the pathogenesis of neurodegeneration in the central nervous system (CNS) [19]. WT and *Ezh2-MKO* mice were then challenged with 6-hydroxydopamine (6-OHDA) to establish a PD-like neurodegeneration model. Interestingly, we observed that *Ezh2* deficiency significantly suppressed NLRP3 inflammasome assembly in microglia located in the striatum, as reflected by dramatically decreased NLRP3 immunofluorescence in Iba1$^+$ microglia (Fig. 2D). Accordingly, decreased microglial NLRP3 inflammasome activation protected dopaminergic neurons from apoptosis/death in the substantia nigra of *Ezh2*-MKO mice (Fig. 2E). Collectively, these data established Ezh2 as a crucial mediator of multiple types of inflammasome activation in both peripheral macrophages and CNS microglia and related pathologies.

Ezh2 mediates lncRNA *Neat1* transcription for inflammasome activation

Since the ASC protein is a shared adaptor and its oligomerization is critical for the assembly and activation of multiple types of inflammasomes, we examined whether Ezh2 modulated ASC oligomerization. The results revealed that *Ezh2* deletion markedly inhibited ASC oligomerization and specks formation through either biochemical or immunofluorescence analysis (Fig. 3A, B). Next, we examined the linear ubiquitination and phosphorylation status of ASC and found that Ezh2 did not affect endogenous ASC linear ubiquitination and phosphorylation in macrophages stimulated with inflammasome inducers (Fig. S3A, B), suggesting that Ezh2 promotes inflammasome activation by modulating ASC oligomerization without affecting its linear ubiquitination and phosphorylation.

Next, we explored whether Ezh2-mediated inflammasome activation was dependent on its methyltransferase activity by using different Ezh2 inhibitors, DZNep and GSK126. Consistent with previous reports, both inhibitors efficiently suppressed Ezh2-mediated H3K27me3 in macrophages; however, DZNep exhibits its function primarily by reducing the Ezh2 protein level, whereas GSK126 directly inhibits its methyltransferase activity without affecting the Ezh2 protein level (Fig. S3C). Interestingly, we found that DZNep obviously inhibited but GSK126 failed to affect caspase-1 cleavage and IL-1β secretion in macrophages induced by nigericin and poly(dA:dT), and a similar phenotype was also observed in microglia treated with DZNep and GSK126 (Fig. 3C–E). In addition, treatment with EED226, an inhibitor of EED, which is a key component of the PRC2 complex, also failed to affect nigericin-induced inflammasome activation (Fig. S3D), suggesting that Ezh2-mediated inflammasome activation is indeed independent of its methyltransferase activity but dependent on its protein level. To identify the functional domain of Ezh2 in modulating inflammasome activation, we generated different domain-truncated Ezh2 expression vectors and then transfected them into HEK293T cells reconstructed with the inflammasome system. The results further confirmed that the SET domain was dispensable for Ezh2-mediated inflammasome activation; however, transfection with an expression plasmid containing the SANT2 domain located between 430 and 500 aa efficiently promoted caspase-1 cleavage, similar to full-length (FL) Ezh2 (Fig. S3E). In contrast, transfection with SANT2-truncated (ΔSANT2) Ezh2 failed to promote caspase-1 cleavage in HEK293T cells (Fig. S3F). Similarly, reconstitution of SANT2-truncated Ezh2 unsuccessfully but FL-Ezh2 or SET-truncated Ezh2 reconstitution successfully rescued nigericin-induced caspase-1 cleavage in *Ezh2*-KO iBMDMs (Fig. 3F). Together, these data suggested that Ezh2 functioned through its SANT2 domain to mediate inflammasome activation independent of its methyltransferase activity.

Inflammasome assembly occurs in the cytosol; however, we observed that Ezh2 expression was maintained in the nucleus with or without inflammasome inducer stimulation (Fig. S3G), implying that Ezh2 indirectly regulates inflammasome activation through an unknown mechanism independent of histone methylation. Because the SANT domain is a highly conserved motif that is similar to Myb DNA-binding domains [20], we performed Ezh2 chromatin immunoprecipitation sequencing (ChIP-seq) to screen for genes with Ezh2 binding ability at the genomic level and then combined these results with our published RNA-seq data [15] to identify genes that both had Ezh2 binding ability and showed

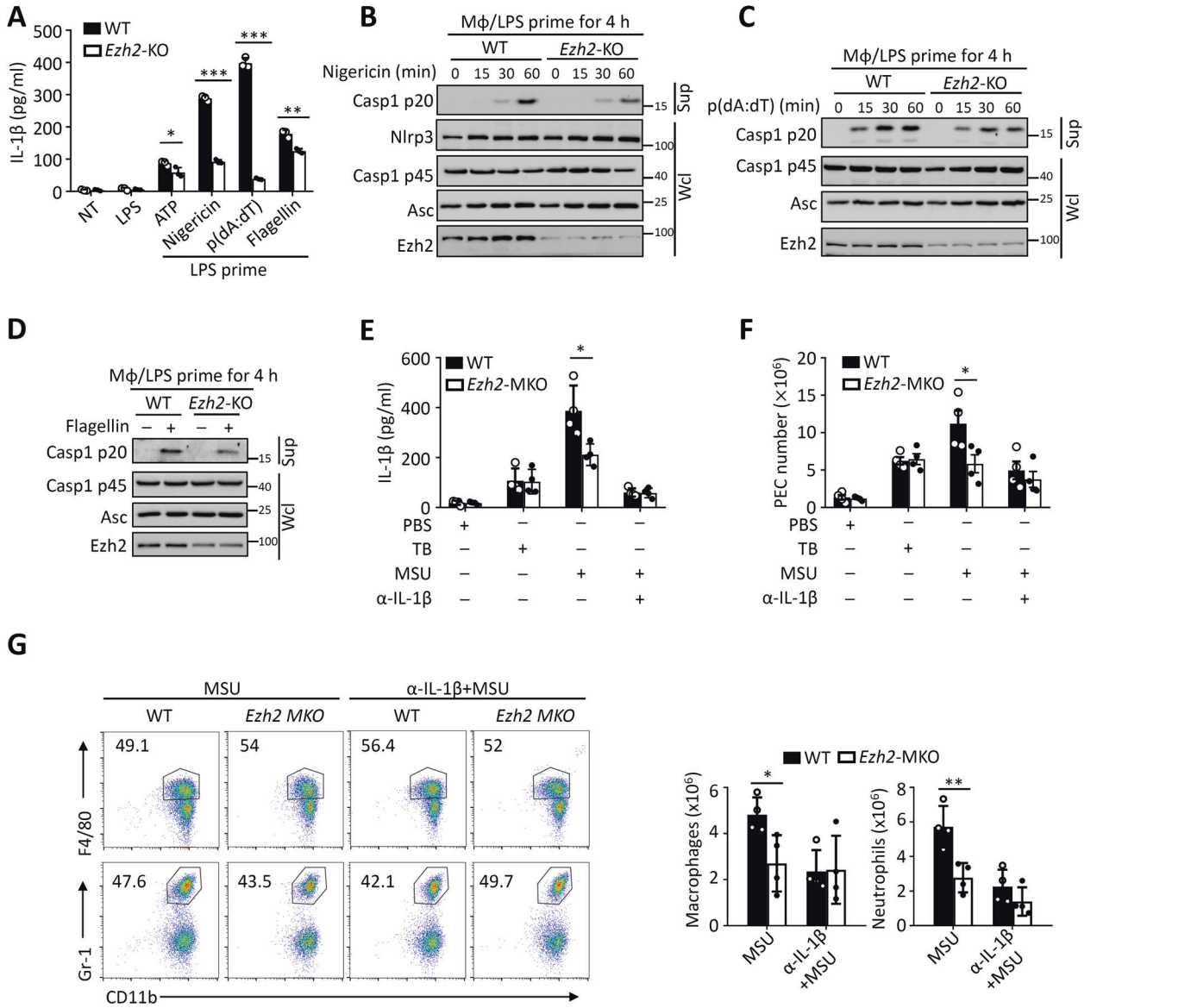

Fig. 1 Ezh2 enhances inflammasome activation in macrophages. A ELISA of IL-1β in culture supernatants from WT and *Ezh2*-KO peritoneal macrophages that were left nontreated (NT), primed with LPS for 4 h, or stimulated with ATP, nigericin, poly(dA:dT) for 1 h or flagellin for 6 h after LPS priming. Immunoblot analysis of caspase-1 processing in the supernatant (Sup) and the whole cell lysates (Wcl) from WT and *Ezh2*-KO macrophages that were primed with LPS for 4 h or stimulated with nigericin (**B**), poly(dA:dT) (**C**) for 1 h or flagellin for 6 h (**D**) after LPS priming. ELISA of IL-1β in peritoneal lavage fluids (**E**) and PEC numbers (**F**) from WT and *Ezh2*-MKO mice that were intraperitoneally injected (i.p.) with PBS, Thioglycolate broth (TB) or MSU for 6 h, or i.p. injected with MSU plus intravenous injection (i.v.) with IL-1β blocking antibody or control antibody, ($n = 4$). **G** Flow cytometric analysis of CD11b$^+$ F4/80$^+$ macrophages and CD11b$^+$ Gr-1$^+$ neutrophils from WT and *Ezh2*-MKO mice that were i.p. injected with MSU 30 min after i.v. injected with IL-1β block antibody or control antibody. Data were presented as flow cytometry plots (**left**) and bar graphs showing absolute cell numbers (**right**), ($n = 4$).

differential expression levels between WT and *Ezh2*-KO macrophages (Fig. 4A). Based on the analysis, we identified seven differentially expressed genes, with the top two hits being *Chil3* and *Neat1*, that had Ezh2-binding ability in macrophages with or without nigericin-induced inflammasome activation (Fig. 4B; Fig. S4A). Since *Chil3* has been reported to solely modulate NLRP3 inflammasome activation without affecting other inflammasomes [21], we focused our following study on *Neat1*, which has been shown to promote NLRP3, NLRC4 and AIM2 inflammasome activation through binding to caspase-1 and stabilising caspase-1 tetramers [8]. This study also showed that *Neat1* knockdown inhibited ASC oligomerization in iBMDMs [8]. Here we confirmed that genetic deficiency of *Neat1* suppressed GSDMD cleavage and ASC oligomerization in primary macrophages (Fig. S4B–D). More importantly, we detected apparent Ezh2 occupancy near the *Neat1* gene transcription start site (Fig. 4C), and ChIP-qPCR analysis showed strong Ezh2 enrichment compared with the immunoglobulin G (IgG) control in the *Neat1* promoter (Fig. 4D). In addition, Ezh2 overexpression greatly enhanced *Neat1* promoter-driven luciferase activity and *Neat1* mRNA levels in primary macrophages, whereas Ezh2 deficiency or knockdown had the opposite effects (Fig. 4E and F; Fig. S4E–G). Moreover, reconstitution of SANT2-truncated Ezh2 unsuccessfully but FL-Ezh2 or SET-truncated Ezh2 reconstitution successfully rescued *Neat1* mRNA expression in *Ezh2*-KO iBMDMs and enhanced *Neat1* promoter-driven luciferase activity in HEK293T cells (Fig. 4G, Fig. S4H). Consistent with these findings, SANT2 domain deletion greatly compromised but SET domain deletion did not affect the binding

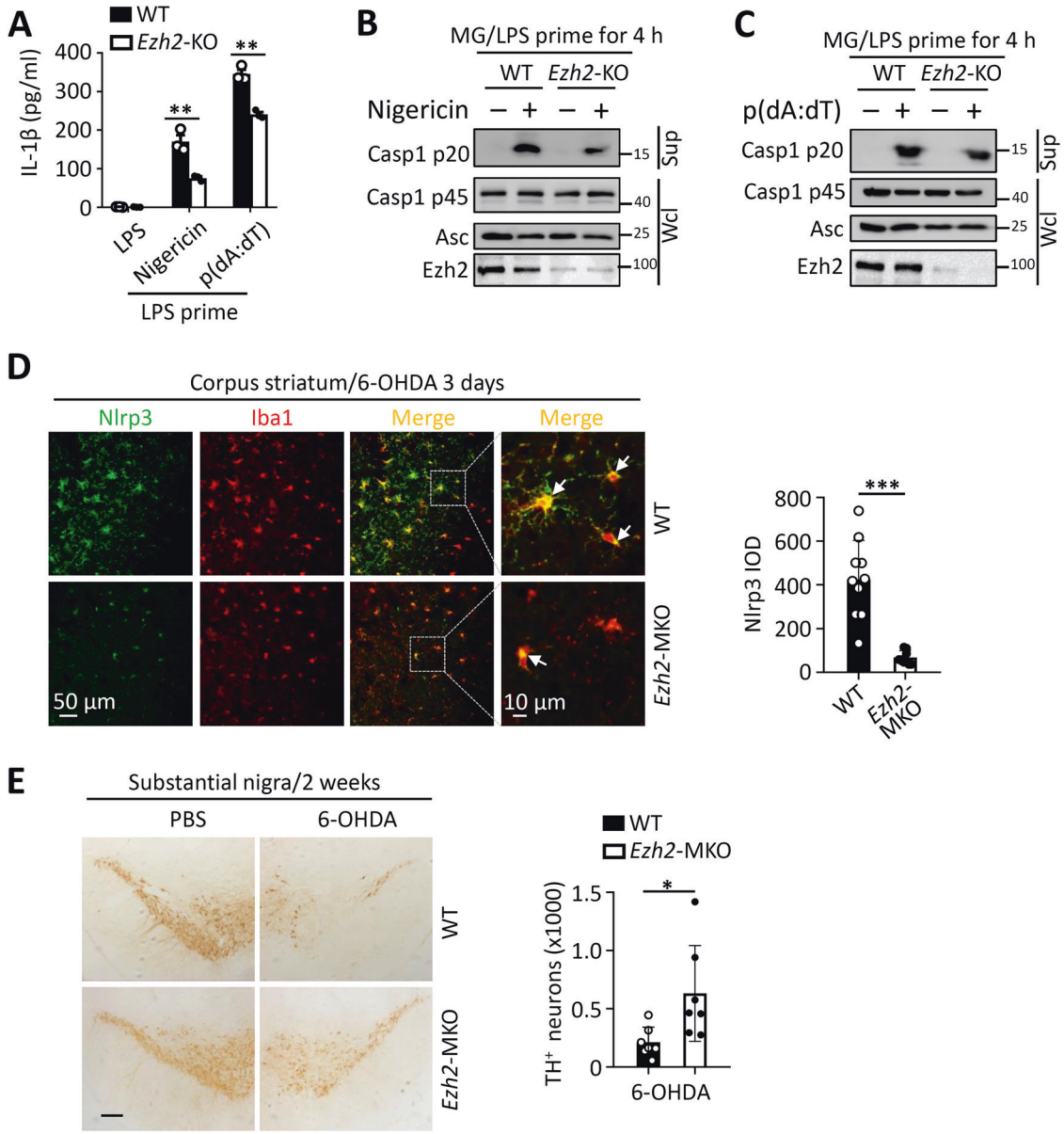

Fig. 2 Ezh2 enhances inflammasome activation in microglia. A ELISA of IL-1β in culture supernatants from WT and *Ezh2*-KO primary microglia that were primed with LPS for 4 h, or stimulated with nigericin or poly(dA:dT) for 1 h after LPS priming. Immunoblot analysis of caspase-1 processing in the supernatant (Sup) and the whole cell lysates (Wcl) from WT and *Ezh2*-KO microglia that were primed with LPS for 4 h or stimulated with nigericin (**B**) or poly(dA:dT) (**C**) for 1 h after LPS priming. **D** Confocal microscopic images (left) and quantification analysis (right) of NLRP3 (green) inflammasome assembly in Iba1$^+$ microglia (red) of striatum from WT and *Ezh2*-MKO mice after unilateral intra-striatal perfusion with 6-OHDA for 3 days. Scale bar, 50 μm and 10 μm ($n = 7$). **E** Immunohistochemical images (left) and quantification analysis (right) of substantia nigra from WT and *Ezh2*-MKO mice after intra-striatal perfusion with PBS or 6-OHDA for 2 weeks. The splices were stained with anti-TH to mark neurons. Scale bar, 250μm, (WT, $n = 10$; *Ezh2*-MKO, $n = 8$).

activity of Ezh2 to the *Neat1* gene promoter (Fig. 4H). In addition, electrophoretic mobility shift assay (EMSA) also confirmed the binding activity between Ezh2 and *Neat1* promoter DNA sequence was dependent on the SANT2 domain (Fig. 4I). These data collectively suggested that Ezh2 was crucial for *Neat1* transcription independent of its methyltransferase activity.

To further confirm that Ezh2-mediated inflammasome activation was dependent on *Neat1*, we manually modulated *Ezh2* and/or *Neat1* expression in iBMDMs and found that knockdown of *Neat1* compromised Ezh2 overexpression-enhanced caspase-1 cleavage in nigericin-stimulated iBMDMs (Fig. S4I, J). In primary macrophages isolated from *Ezh2*- and/or *Neat1*-KO mice, genetic ablation of *Ezh2* or *Neat1* alone suppressed caspase-1 cleavage and IL-1β secretion stimulated with either nigericin or poly(dA:dT), and Ezh2/Neat1 double deficiency did not further inhibit inflammasome activation-induced caspase-1 cleavage and IL-1β secretion (Fig. 4J, L). Inversely, overexpression of *Neat1* rescued the inhibition of caspase-1 cleavage in *Ezh2*-deficient iBMDM (Fig. 4, K; Fig. S4K). Accordingly, this phenotype was also confirmed in the MSU-challenged mouse model, as reflected by no significant difference in IL-1β secretion and PEC numbers between *Ezh2*-KO, *Neat1*-KO and *Neat1*/*Ezh2* double KO mice (Fig. 4M; Fig. S4L). Interestingly, we observed the *NEAT1* gene expression in PD patients was higher than that in healthy people (Fig. S4M), which is in consistent with *EZH2* expression pattern. Collectively, these data suggested that Ezh2-mediated

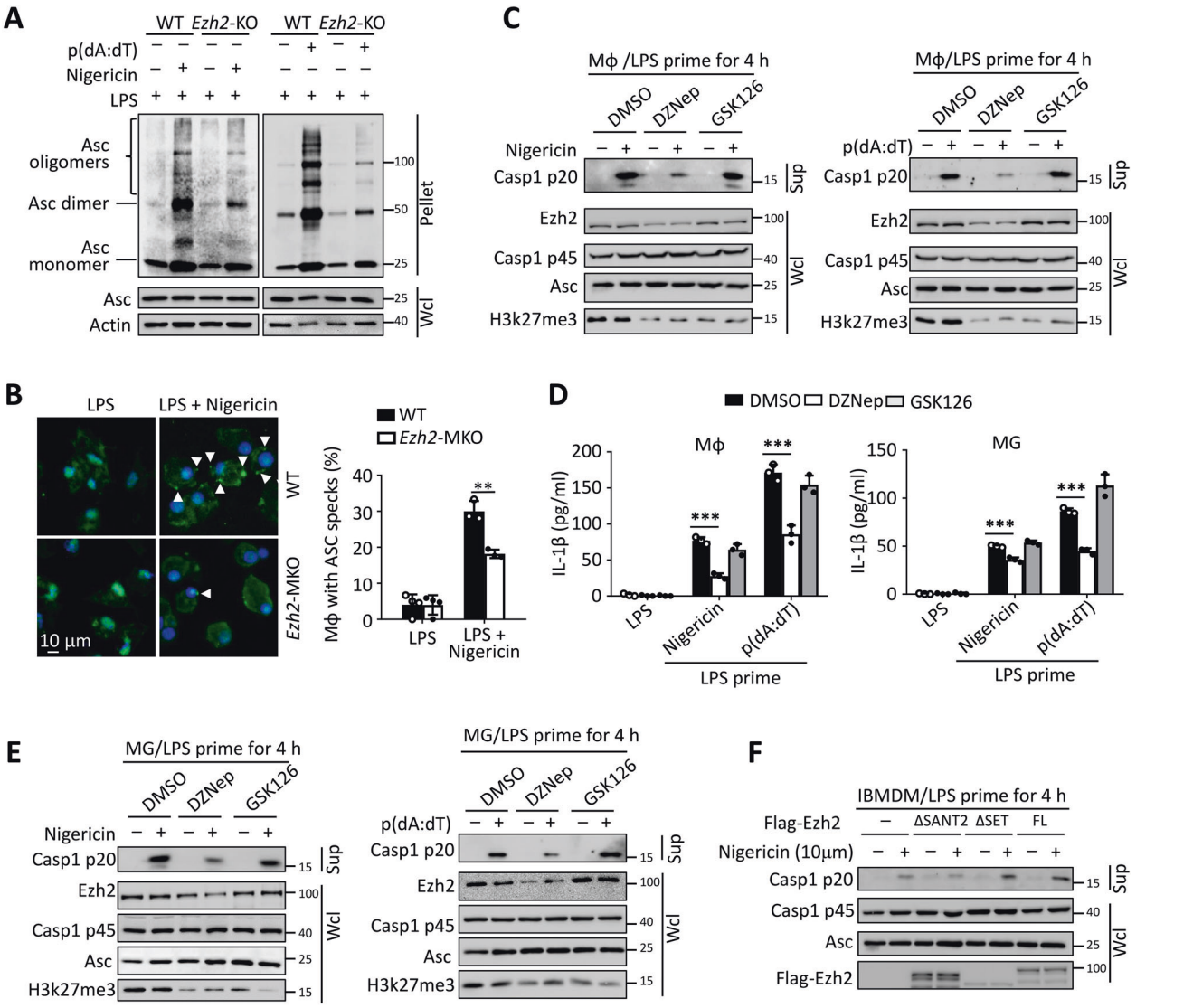

Fig. 3 Ezh2 facilitates inflammasome activation through its SANT2 domain and independent of its methyltransferase activity. **A** Immunoblot analysis of ASC oligomerization in the pellet and Wcl from WT and *Ezh2*-KO macrophages that were primed with LPS for 4 h or stimulated with nigericin and poly(dA:dT) for 1 h after LPS priming. **B** Confocal microscopic images (left) and quantification analysis (right) of ASC specks (green) from WT and *Ezh2*-KO macrophages that were primed with LPS for 4 h or stimulated with nigericin for 1 h after LPS priming. Scale bar, 10 μm. Immunoblot analysis of caspase-1 processing and IL-1β ELISA in the supernatant (Sup) and the whole-cell lysates (Wcl) from macrophages (*Mφ*, **C**, **E**) or microglia (MG, **D**, **E**) that were pretreated with DMSO, DZNep (5 μM) or GSK126 (5 μM) for 72 h, then stimulated with nigericin (left) or poly(dA:dT) (right) for 1 h after LPS priming. **F** Immunoblot analysis of caspase-1 processing in the supernatant (Sup) and the whole-cell lysates (Wcl) from *Ezh2*-KO iBMDMs that were reconstituted with empty vector (-), full-length (FL) Ezh2, SANT2-truncated (ΔSANT2) or SET-truncated (ΔSET) Ezh2, and then were primed with LPS for 4 h or stimulated with nigericin for 1 h after LPS priming.

inflammasome activation was indeed dependent on its transcriptional activation of lncRNA *Neat1*.

Ezh2 maintains H3K27ac in the *Neat1* promoter by inhibiting SIRT1-mediated deacetylation

The biological function of Ezh2 is mainly focused on its transcriptional inhibition of gene expression through H3K27me3. A recent study demonstrated that EZH2 directly binds to the promoter of the androgen receptor gene, which is associated with enriched H3K27 acetylation (H3K27ac) in its promoter region, and thus promots its transcriptional activation in prostate cancer cells [22]. We, therefore, examined whether Ezh2-mediated transcriptional activation of *Neat1* was also associated with enriched H3K27ac in macrophages through combined ChIP-seq of H3K27ac, H3K27me3 and Ezh2 at the genome level. Combined with previous analysis of Ezh2 binding genes, the Venn diagram revealed that 3149 (51%) and 1550 (25%) Ezh2-binding genes were occupied by H3K27me3 and H3K27ac, respectively (Fig. 5A), suggesting that most of the Ezh2-binding genes were associated with H3K27me3-mediated transcriptional suppression, whereas approximately one-fourth of the Ezh2-binding genes were associated with H3K27ac-related transcriptional activation. Among these Ezh2-binding genes, the H3K27ac and H3K27me3 binding sites were almost reciprocally exclusive (Fig. 5B). Interestingly, we found that the *Neat1* gene promoter was strongly occupied by H3K27ac but not H3K27me3 (Fig. 5C). Moreover, ChIP-qPCR analysis revealed that *Ezh2* deletion impaired but *Ezh2* overexpression greatly enhanced the enrichment of H3K27ac in the *Neat*1 gene promoter (Fig. 5D, E). These results collectively suggested that

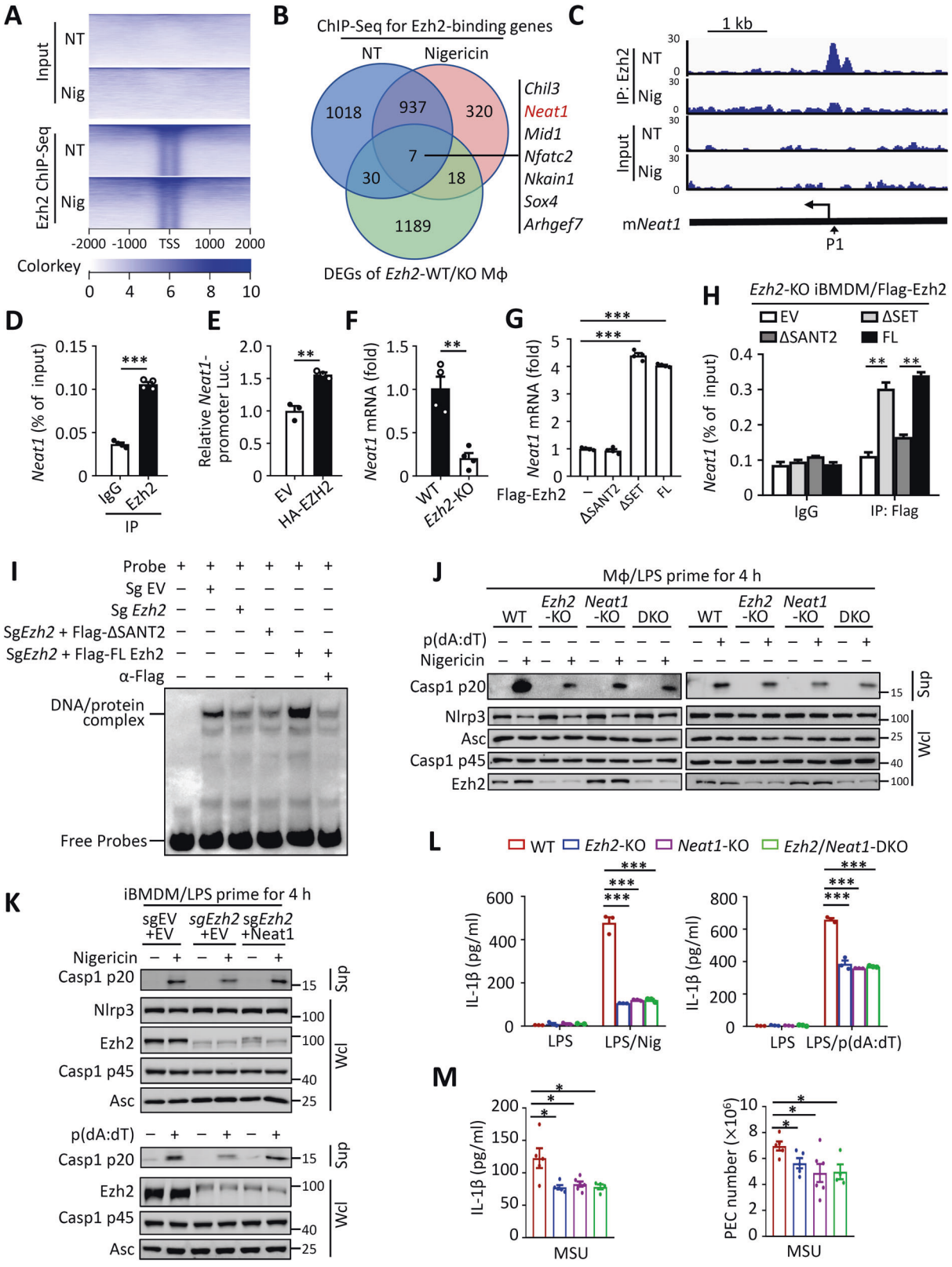

Ezh2 mediated *Neat1* transcription by maintaining H3K27ac in the promoter of *Neat1*.

To determine how Ezh2-maintained H3K27ac promoted *Neat1* transcription, we examined *Neat1* promoter-driven luciferase activity in HEK293T cells transfected with different histone acetyltransferases, histone deacetylases (HDACs) or sirtuin (SIRT) family deacetylases. Interestingly, we found that overexpression of the deacetylase SIRT1 prominently inhibited *Neat1* transcriptional activity (Fig. 5F), whereas knockdown of *SIRT1* greatly upregulated *Neat1* transcription in iBMDMs (Fig. 5G and Fig. S5A, B). In

Fig. 4 Ezh2 mediates lncRNA *Neat1* transcription for inflammasome activation. A The heatmap of input and Ezh2 ChIP-Sequencing signals at transcription start site (TSS) (±2 kb) in primary macrophages that were left nontreated (NT) or stimulated with nigericin for 1 h after LPS priming (Nig). **B** Venn diagram showing overlap genes among the differentially expressed genes (DEGs) of *Ezh2*-WT/KO macrophages, Ezh2-binding genes in macrophages that were left nontreated (NT) or stimulated with nigericin for 1 h after LPS priming. **C** Snapshot of the Ezh2 ChIP-Seq signals at the *Neat1* gene loci in macrophages that were nontreated (NT) or stimulated with nigericin after LPS priming; the arrow indicated the location of the ChIP-qPCR primers. **D** ChIP-qPCR analysis of Ezh2 binding to the promoters of *Neat1* gene. **E** *Neat1* promoter-driven luciferase activity in HEK293T cells transfected with empty vector (EV) or HA-EZH2. QPCR analysis of *Neat1* mRNA in WT and *Ezh2*-KO macrophages (**F**), or in *Ezh2*-KO iBMDMs reconstituted with empty vector (-), FL-Ezh2, Ezh2-ΔSANT2 and Ezh2-ΔSET (**G**). **H** ChIP-qPCR analysis of the binding activity of full-length (FL) or truncated Ezh2 to the promoters of *Neat1* gene. **I** Electrophoretic mobility-shift assay (EMSA) of the binding activities of full-length (FL) or truncated Ezh2 to the DNA probes based on mouse *Neat1* gene promoters DNA sequence. The nuclear proteins were extracted from WT iBMDMs that transfected with sgEV and *Ezh2*-KO iBMDMs (sg*Ezh2*) that were reconstituted with full-length Flag-Ezh2 (sg*Ezh2* + Flag-FL Ezh2) or SANT2-truncated Ezh2 (sg*Ezh2* + Flag-ΔSANT2). **J** Immunoblot analysis of caspase-1 processing in the supernatant (Sup) and the whole-cell lysates (Wcl) from WT, *Ezh2*-KO, *Neat1*-KO and *Ezh2/Neat1* double KO (DKO) macrophages that were primed with LPS for 4 h or stimulated with nigericin or poly(dA:dT) for 1 h after LPS priming. **K** Immunoblot analysis of caspase-1 processing in the supernatant (Sup) and the whole-cell lysates (Wcl) from control (sgEV + EV), *Ezh2*-KO iBMDMs reconstituted with empty vector (sg*Ezh2* + EV) or *Neat1* expression vector (sg*Ezh2* + *Neat1*). The cells were primed with LPS and then left unstimulated or stimulated with nigericin or poly(dA:dT) after LPS priming. **L** ELISA of IL-1β in the supernatant (Sup) from WT, *Ezh2*-KO, *Neat1*-KO and *Ezh2/Neat1* double KO (DKO) macrophages that were primed with LPS for 4 h or stimulated with nigericin or poly(dA:dT) for 1 h after LPS priming. **M** PEC number and ELISA of IL-1β in peritoneal lavage fluids from WT, *Ezh2*-KO, *Neat1*-KO and *Ezh2/Neat1* double KO (DKO) mice i.p. injected with MSU for 6 h, each dot represented a mouse.

addition, the NAD^+ modulators like nicotinamide mononucleotide (β-NM) or nicotinamide riboside (NR), which could restore SIRT1 activity, also decreased *Neat1* mRNA expression (Fig. S5C). All of these results suggested that SIRT1 might regulate *Neat1* transcription by modulating the acetylation status at H3K27 of the *Neat1* promoter. As expected, reducing SIRT1 expression significantly increased H3K27ac levels in the *Neat1* promoter and obviously promoted caspase-1 cleavage upon nigericin and poly (dA:dT) stimulation (Fig. 5H, I). In addition, although Ezh2 did not affect SIRT1 expression (Fig. S5D), ChIP-seq results revealed that its deficiency significantly increased the binding of SIRT1 in the genome of primary macrophages (Fig. S5E, F). Regarding the *Neat1* gene, *Ezh2* deletion notably increased the occupancy of SIRT1 in the promoter region, which was further validated by ChIP-qPCR results (Fig. 5J, K). Additionally, the selective SIRT1 inhibitor EX527 dramatically enhanced *Neat1* mRNA expression in *Ezh2*-deficient primary macrophages and eliminated the difference in *Neat1* transcription between WT and *Ezh2*-KO macrophages (Fig. 5L). Therefore, our data suggested that Ezh2 maintains H3K27ac occupancy in the *Neat1* promoter by suppressing SIRT1-mediated deacetylation, thereby promoting *Neat1* transcription and inflammasome activation.

Generally, histone lysine acetylation is associated with an active chromatin state for recruiting transcription factors to initiate gene expression [23, 24]. To confirm that Ezh2-mediated *Neat1* transcription is associated with H3K27ac-induced increased chromatin accessibility in the *Neat1* gene promoter, we performed ATAC-seq on the chromatin of WT and *Ezh2*-KO macrophages and found that *Ezh2* deficiency obviously decreased chromatin accessibility in the *Neat1* promoter (Fig. 6A). Next, we screened for potential transcription factors of the *Neat1* gene based on published studies by examining their effect on *Neat1* promoter-driven luciferase activity [25–27]. The results revealed that p65 robustly promoted *Neat1* transcriptional activity (Fig. 6B). Accordingly, the ChIP-seq data confirmed that p65 was strongly recruited to the *Neat1* promoter in macrophages (Fig. 6C) [28]. In addition, in the *Neat1* gene promoter region, we observed similar peak patterns by comparing the H3K27ac ChIP-seq data with the ATAC-seq data, and the peaks of p65 enrichment were located exactly at the accessible region of chromatin (Fig. 6D). Meanwhile, a conserved p65-binding motif was identified at −428 to −418 of the *Neat1* gene promoter region (Fig. 6E). Moreover, *Ezh2* deficiency largely suppressed p65 enrichment (Fig. 6F), whereas downregulation of SIRT1 significantly promoted p65 occupancy in the *Neat1* promoter (Fig. 6G). Furthermore, reducing *p65* expression significantly suppressed *Neat1* transcription and compromised Ezh2 overexpression-enhanced *Neat1* transcription (Fig. 6H, I), which suggested that Ezh2-mediated *Neat1* transcription is dependent on the accessibility of p65 in its promoter region. Together, these data demonstrated that Ezh2-maintained H3K27ac in the *Neat1* gene promoter facilitates p65-mediated transcriptional activation of *Neat1*.

Ezh2 excludes p53 to allow *Neat1* transcription

To determine how Ezh2 suppressed SIRT1 occupancy in the *Neat1* promoter, we performed mass spectrometry analysis to screen potential SIRT1-associated chromatin DNA-binding proteins. Among the top identified hits, according to previous reports, p53 could bind to the promoter region of NEAT1 in human breast cancer and pancreatic cancer cell lines [29, 30]. Even more importantly, a published study reported that p53 could interact with SIRT1 closely [31]. Therefore, p53 was selected for further investigation (Fig. S6A). Immunoblotting confirmed the binding of p53 with SIRT1 both in the HEK293T overexpression system and in primary macrophages, and their interaction was independent of Ezh2, which did not bind to SIRT1 (Fig. S6B and C). Interestingly, *Neat1* mRNA expression was increased when *p53* was knocked down in iBMDMs (Fig. S6D). To investigate whether p53 modulated SIRT1 occupancy and then *Neat1* expression, we generated myeloid cell *p53* conditional KO (*p53*-MKO) mice. Consistent with the *p53* knockdown results, *p53* deletion in macrophages prominently enhanced *Neat1* transcription (Fig. 7A). In contrast, treatment with nutlin-3, an inhibitor of the MDM2-p53 interaction, dramatically stabilised p53 protein expression and then inhibited *Neat1* mRNA expression accordingly (Fig. S6E and Fig. 7B). Although p53 was dispensable for Sirt1 mRNA expression (Fig. S6F), *p53* deletion impaired SIRT1 binding across the whole genome in primary macrophages (Fig. S6G and H). In the *Neat1* gene promoter region, SIRT1 occupancy was sharply reduced with *p53* deficiency, and this result was confirmed by ChIP-qPCR assay (Fig. 7C, D). Accordingly, *p53* deficiency notably enhanced the H3K27ac level in the *Neat1* gene promoter, resulting in a loose chromosome structure for p65 recruitment to mediate *Neat1* transcription (Fig. 7E–G). Furthermore, we also found *p53* deficiency promoted caspase-1 cleavage and increased the production of N-terminal of GSDMD in primary macrophages induced by nigericin and poly(dA:dT) (Fig. S6I–K). These data suggested that p53 is critical for the recruitment of SIRT1 to inhibit H3K27ac in *Neat1* gene promoter and thus suppress inflammasome activation.

To further confirm the role of p53 in recruiting SIRT1 for H3K27 deacetylation, human THP-1 cells, which has a deletion in *p53* coding sequence leading to loss of *p53* expression, were applied for the experiments [32]. We found that knockdown of *Neat1* also

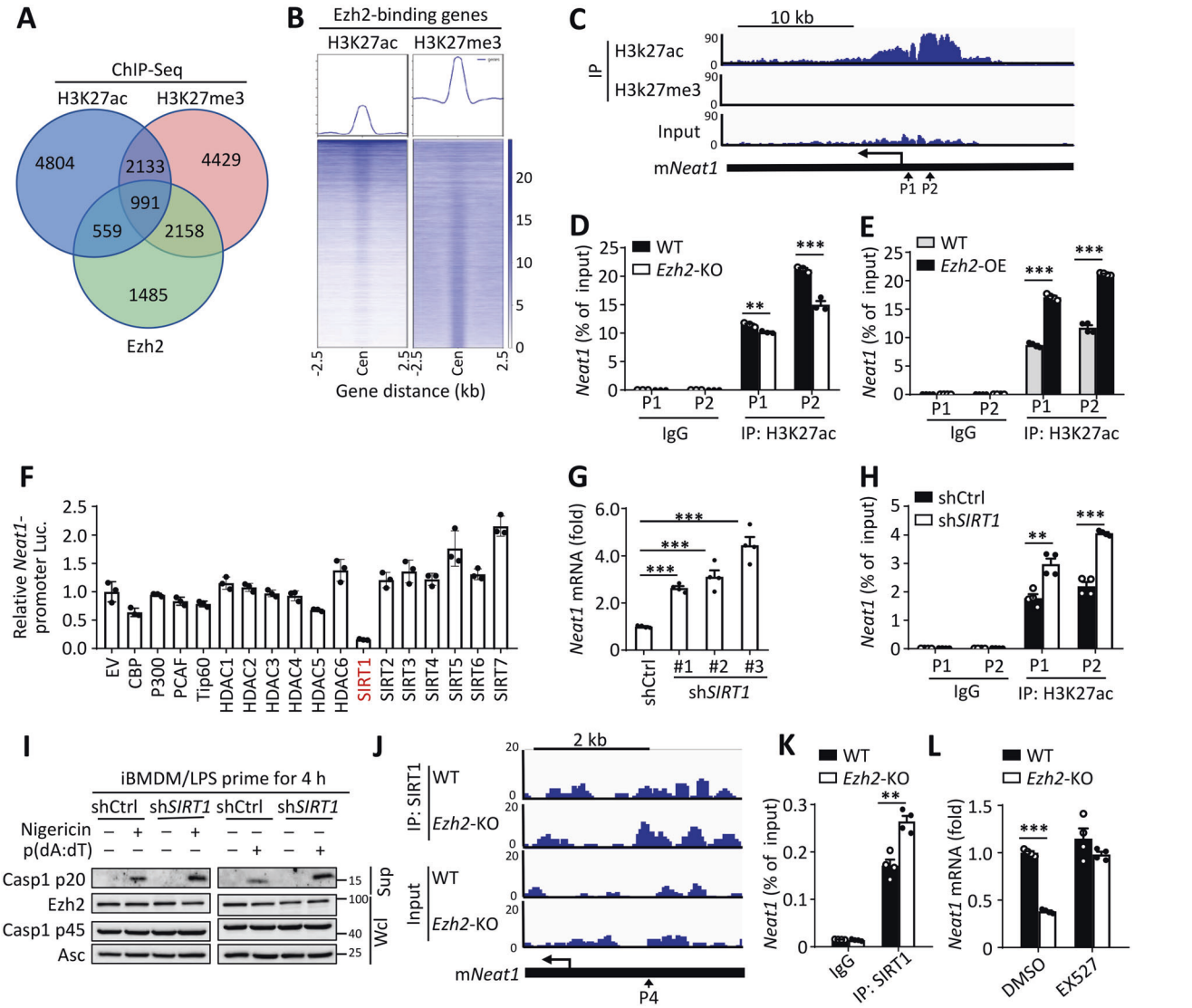

Fig. 5 Ezh2 maintains H3K27ac in *Neat1* promoter by inhibiting SIRT1-mediated deacetylation. A Venn diagram showing overlap gene numbers among Ezh2-binding genes and genes with H3K27ac or K3K27me3 marks in primary macrophages based on ChIP-seq analysis. **B** The average intensities (upper) and heatmap (lower) of H3K27ac and H3K27me3 marks restricted in all Ezh2-binding genes. **C** Snapshot of the H3K27ac and H3K27me3 ChIP-Seq signals at the *Neat1* gene loci. ChIP-QPCR analysis of the H3K27ac level at the *Neat1* gene promoter of in WT and *Ezh2*-KO macrophages (**D**) or in WT and *Ezh2*-overexpression (OE) iBMDMs (**E**). **F** *Neat1* promoter-driven luciferase activity in HEK293T cells transfected with different expression vectors encoding histone acetyltransferases (CBP, P300, PCAF, and Tip60), histone deacetylases (HDAC1-HDAC6) and SIRT family of deacetylases (SIRT1-SIRT7). **G** QPCR analysis of *Neat1* mRNA in control (shCtrl) and *SIRT1* knockdown (sh*SIRT1* #1, #2 and #3) iBMDMs. **H** ChIP-QPCR analysis of H3K27ac signal at the *Neat1* gene promoters in control (shCtrl) and *SIRT1*-knockdown (sh*SIRT1*) iBMDMs. **I** Immunoblot analysis of caspase-1 processing in the supernatant (Sup) and the whole cell lysates (Wcl) from control and *SIRT1*-knockdown iBMDMs that were primed with LPS for 4 h, or stimulated with nigericin (left) and poly (dA:dT) for 1 h after LPS priming (right). **J** Snapshot of the SIRT1 ChIP-Seq signals at the *Neat1* gene loci in WT and *Ezh2*-KO macrophages; the arrows indicated the location of the ChIP-QPCR primers. **K** ChIP-QPCR analysis of SIRT1 binding to the promoter of Neat1 in WT and *Ezh2*-KO macrophages. **L** QPCR analysis of *Neat1* mRNA in WT and *Ezh2*-KO macrophages pretreated with DMSO or EX527 (10 μM) for 72 h.

suppressed NLRP3 inflammasome activation and downstream IL-1β production in THP-1 cells (Fig. S6L–N). ChIP-seq analysis showed that no SIRT1 occupation but strong H3K27ac enrichment was observed in the promoter region of human *NEAT1* gene in THP-1 cells (Fig. 7H). In addition, overexpression of p53 in THP-1 cells significantly promoted SIRT1 enrichment whereas suppressed H3K27ac signal in human *NEAT1* gene promoter (Fig. 7I, J; Fig. S6O). Accordingly, p53 overexpression could obviously inhibit *NEAT1* mRNA expression, and thus the caspase-1 cleavage and IL-1β secretion in THP-1 cells (Fig. 7K; Fig. S6P, Q). These data confirmed the regulatory mechanism that p53 acting through recruitment of SIRT1 to reduce histone acetylation for *NEAT1* gene suppression in human-derived THP-1 cells, which is in consistent with the mechanism identified in mouse macrophages.

Considering the opposite effects of Ezh2 and p53 on modulating SIRT1-mediated H3K27 deacetylation and *Neat1* expression, we speculated that Ezh2 might eliminate p53 occupancy to allow *Neat1* transcription. Interestingly, ChIP-seq results showed that Ezh2 and p53 bound to the same site of the *Neat1* gene promoter in primary macrophages (Fig. 7L). EMSA showed that nutlin-3 treatment markedly promoted the formation of DNA/protein complex (Fig. S6R), which confirmed the binding of p53 in *Neat1* gene promoter. In addition, deletion of either *Ezh2* or *p53* suppressed the formation of DNA/protein complex at the same

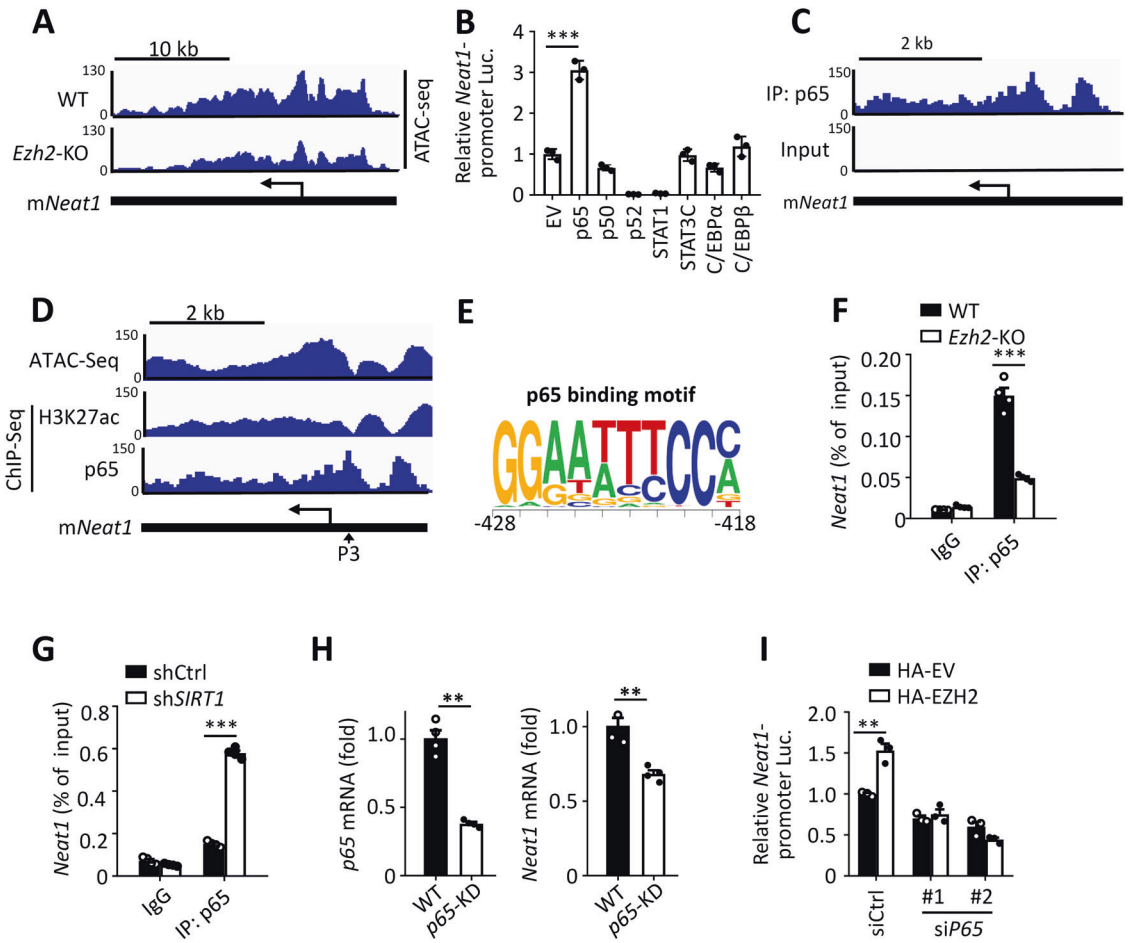

Fig. 6 Ezh2-mediated *Neat1* transcription is dependent on p65. A Snapshot of the ATAC-seq signals at the *Neat1* gene loci in WT and *Ezh2*-KO macrophages. **B** *Neat1* gene promoter-driven luciferase activity in HEK293T cells transfected with expression vector encoding p65, p50, p52, STAT1, STAT3C, C/EBPα and C/EBPβ. **C** Snapshot of the p65 ChIP-Seq signals at the *Neat1* gene loci in macrophages that were nontreated. **D** Comparison of the H3K27ac and p65 ChIP-seq signals with ATAC-seq signals at *Neat1* gene loci in primary macrophages, the arrows showed the location of the ChIP-QPCR primers. **E** The conserved p65 binding motif is located in the promoter region of mouse *Neat1* gene loci between −428 and −418 bp. ChIP-QPCR analysis of p65 binding to the *Neat1* gene promoter in WT and *Ezh2*-KO macrophages (**F**) or in the control and *SIRT1*-knockdown iBMDMs (**G**). **H** QPCR analysis of *p65* and *Neat1* mRNA in WT and *p65*-knockdown Raw264.7 cells. **I** *Neat1* promoter-driven luciferase activity in HEK293T cells transfected with control siRNA or *p65*-targeted siRNA (si*p65* #1 and #2) for 24 h and then transfected with empty vector (EV) or HA-EZH2.

location of the EMSA band, and *Ezh2*/*p53* double-KO almost abolished the DNA/protein complex formation also at the same EMSA band location (Fig. S6S), suggesting that p53 and Ezh2 indeed could bind to the same DNA sequence of *Neat1* gene promoter. However, EMSA could not distinguish the interaction band between p53/DNA and Ezh2/DNA, possibly due to the excessive presence of DNA probes in the EMSA experiment.

To examine the competition for binding to *Neat1* promoter between Ezh2 and p53, we applied ChIP-QPCR experiment that can detect the physiological interaction between nuclear proteins and genomic DNA without adding large amount of DNA probes. The results showed that Ezh2 overexpression significantly inhibited p53 binding, whereas *Ezh2* deficiency markedly promoted p53 recruitment to the *Neat1* gene promoter (Fig. 7M, N). Likewise, *p53* deletion promoted Ezh2 occupancy, whereas nutlin-3-induced *p53* overexpression suppressed Ezh2 binding in the *Neat1* gene promoter (Fig. 7O, P). These results implied that Ezh2 excluded p53 to bind to the *Neat1* gene promoter region. Functionally, overexpression of *p53* compromised *Ezh2* overexpression-enhanced *Neat1* promoter-driven luciferase activity in HEK293T cells (Fig. 7Q), and *p53* deletion antagonised *Ezh2* deficiency-induced downregulation of *Neat1* expression in primary macrophages (Fig. S6T). Accordingly, *Ezh2* deficiency failed to inhibit caspase-1 cleavage and IL-1β secretion when *p53* was deleted in primary macrophages stimulated with nigericin or poly (dA:dT) (Fig. 7R–T). Together, these data demonstrated that the Ezh2/p53/Sirt1 axis modulated *Neat1* transcription for inflammasome activation.

DISCUSSION

Histone lysine modification status is delicately regulated by different lysine modification enzymes, which play a crucial role in the epigenetic regulation of gene expression [33, 34]. Ezh2 is a well-characterised histone lysine methyltransferase that mainly mediates H3K27me3 for gene transcriptional repression, especially in tumour biology [35]. We also confirmed that the majority of Ezh2-binding genes were associated with H3K27me3 in macrophages through ChIP-seq analysis. However, our current study found that Ezh2, rather than a methyltransferase that mediates H3K27me3 for gene repression, promoted lncRNA *Neat1* transcription for inflammasome activation. This gene transcriptional activating role of Ezh2 was associated with high levels of H3K27ac to loosen the chromatin structure in the *Neat1* gene

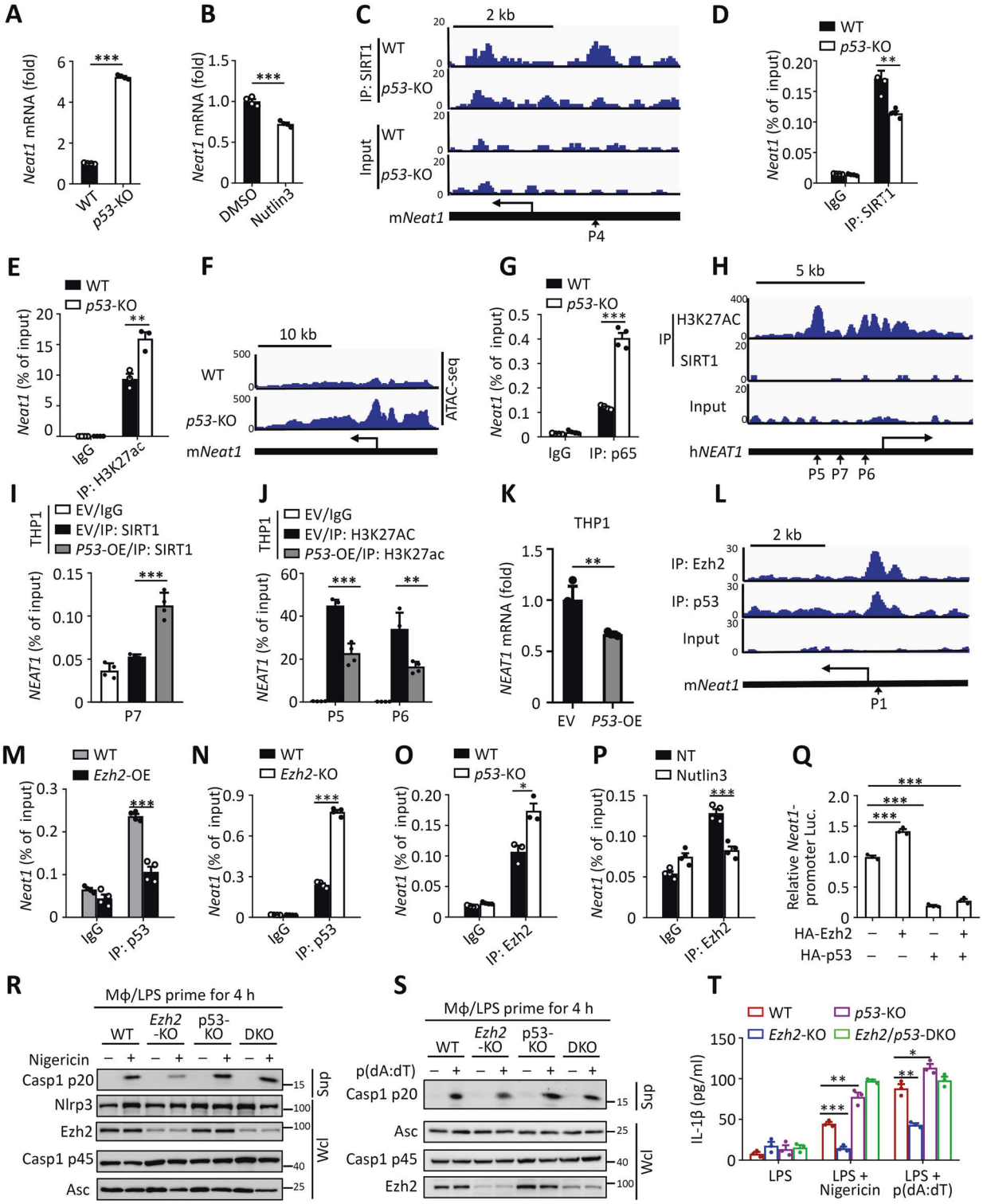

promoter. Our ChIP-seq data also confirmed that approximately one-fourth of Ezh2-binding genes were associated with H3K27ac, implying that this gene-promoting function of Ezh2 might be universal across the genome. Although a recent study suggested that *Ezh2* expression is associated with high levels of H3K27ac to promote androgen receptor gene transcription in a methyltransferase- and PRC2-independent manner in prostate cancer [36], the molecular mechanism of Ezh2 in promoting H3K27ac to support gene transcription is not clear. Here, we also identified that the deacetylase SIRT1 was a critical negative regulator of Ezh2-maintained H3K27ac, and *Ezh2* deficiency greatly increased SIRT1-mediated H3K27 deacetylation at the *Neat1* promoter, thereby inhibiting *Neat1* transcription. However, how H3K27ac is established in *Neat1* and other Ezh2-activated genes still needs further investigation. Moreover, our ChIP-seq data also found a large number of Ezh2-binding genes that were associated with neither

Fig. 7 Ezh2 excludes p53 to allow *Neat1* transcription. QPCR analysis of *Neat1* mRNA in WT and *p53*-KO macrophages (**A**) and in macrophages pretreated with DMSO or Nutlin3 (10 μM) for 24 h (**B**). **C** Snapshot of the SIRT1 ChIP-Seq signals at the *Neat1* gene loci in WT and *p53*-KO macrophages. ChIP-QPCR analysis of SIRT1 (**D**), H3K27ac (**E**) and p65 (**G**) signals in the *Neat1* gene promoter, and Snapshot of the ATAC-seq signals at the mouse *Neat1* gene loci in WT and *p53*-KO macrophages (**F**). **H** The snapshot of the H3K27ac and SIRT1 ChIP-Seq signals at the human *NEAT1* gene loci inTHP-1 cells. ChIP-QPCR analysis of SIRT1 (**I**) and H3K27ac (**J**) binding to the human *NEAT1* gene promoter (**I** and **J**), and QPCR analysis of *NEAT1* mRNA (**K**) in THP-1 cells that reconstituted with empty vector (EV) or *P53*-overexpression (OE) vector. **L** Comparison of the snapshot of the Ezh2 and p53 ChIP-Seq signals at the *Neat1* gene loci in macrophages. ChIP-QPCR analysis of p53 binding to the *Neat1* gene promoter in WT and *EZH2*-overexpression (OE) iBMDMs (**M**), and in WT and *Ezh2*-KO macrophages (**N**). ChIP-QPCR analysis of Ezh2 binding to the *Neat1* gene promoter in WT and *p53*-KO macrophages (**O**), and macrophages pretreated with DMSO or Nutlin3 (10 μM) for 24 h (**P**). **Q** *Neat1* promoter-driven luciferase activity in HEK293T cells transfected with HA-EZH2 and/or HA-P53. Immunoblot analysis of caspase-1 processing in the supernatant (Sup) and the whole cell lysates (Wcl) (**R**, **S**) and ELISA of IL-1β in culture supernatant (**T**) from WT, *Ezh2*-KO, *p53*-KO and *Ezh2*/*p53* double KO (DKO) macrophages primed with LPS for 4 h or stimulated with nigericin (**R**) and poly (dA:dT) (**S**) for 1 h after LPS priming.

H3K27me3 nor H3K27ac, suggesting a unique H3K27me3- and H3K27ac-independent role of Ezh2 in regulating gene expression, which also needs further investigation.

In addition to tumour biology, others and our group had reported that Ezh2 functioned in multiple types of immune cells to modulate the pathogenesis of many inflammatory diseases, such as colitis, multiple sclerosis and lupus-like disease [15, 37, 38]. Similar to Ezh2, lncRNA *Neat1* also had been reported to play a crucial role in inflammatory diseases. For instance, *NEAT1* expression was abnormally increased in systemic lupus erythematosus, and silencing *NEAT1* significantly reduced LPS-induced expression of chemokines and cytokines [39]. Neat1 had also been reported to promote rheumatoid arthritis pathogenesis [40]. A recent study has shown that *Neat1* is a critical mediator for multiple types of inflammasome activation, and knockdown of *Neat1* greatly suppressed ASC oligomerization in iBMDM [8]. Our study also confirmed that *Neat1* deficiency in primary macrophages also inhibited the ASC oligomerization and thus inflammasome activation, which is in concert with Ezh2 function. It is noteworthy that the relationship between Ezh2 and *Neat1* is complicated. In muscle cells, *Neat1* physically interact with Ezh2 and recruit Ezh2 to target gene promoters [41]. Our study further clarified their relationship in the context of inflammasome activation in macrophages.

The SET domain is critical for Ezh2-mediated methyltransferase activity to establish H3K27me3 for gene repression. Targeting SET-mediated methyltransferase activity through the selective inhibitor GSK126 has been applied in clinical trials for the treatment of patients with multiple types of tumours [14, 42, 43]. Here, we found that Ezh2-mediated *Neat1* transcription and inflammasome activation were independent of its SET domain in macrophages, as confirmed by SET domain deletion or GSK126 treatment, but required its chromatin DNA-binding SANT2 domain. Although SANT domain-mediated DNA binding activity has been reported in some SANT-containing proteins [44, 45], the biological function of SANT2 in the Ezh2 protein has not been uncovered. Our study provided evidence that SANT2 domain deletion greatly suppressed Ezh2-mediated *Neat1* transcription and subsequent inflammasome activation, which revealed a previously unidentified novel function of Ezh2. Therefore, the development of SANT2-targeted Ezh2 inhibitors may have therapeutic potential for inflammasome-dependent inflammatory diseases.

Both Ezh2 and p53 are key modulators in cancer biology; however, their relationship remains undetermined. We also noted that Ezh2 deficiency could downregulate miR-375 in breast cancer, thereby increasing p53 expression [46]. However, our data showed that Ezh2 did not affect p53 expression in macrophages, which means that miR-375 may not be involved in this process. Interestingly, previous studies have shown that NEAT1, as a transcriptional target of p53, plays a tumour suppression role in tumour cell lines [29, 30]. In contrast, we found that p53 deficiency could increase the expression of NEAT1 in macrophages. It is possible that a different interaction between p53 and NEAT1 exists in tumour cells and immune cells. Here, we proposed a model in which Ezh2 shares a binding site with p53 in the *Neat1* promoter and eliminates p53 occupancy to modulate *Neat1* transcription and inflammasome activation. As a result, *Ezh2* deficiency greatly increases the occupancy of p53, which then recruits SIRT1 to mediate H3K27 deacetylation in the *Neat1* promoter, thereby inhibiting *Neat1* transcription and inflammasome activation. However, Ezh2 deletion failed to inhibit p53 deficiency-enhanced *Neat1* transcription and inflammasome activation, suggesting that p53 deficiency dominantly regulates inflammasome activation independent of Ezh2. The inflammasome-activating effect of p53 deficiency may also explain recently published data showing that myeloid cell p53 deletion promotes inflammation-induced colon tumorigenesis [47]. In addition, our proposed Ezh2/p53/Sirt1 axis might also modulate the expression of genes other than *Neat1*. Moreover, recent studies have suggested that inflammasome-induced pyroptosis is widely involved in multiple cancers, such as gastric cancer and breast cancer [48–50]. Therefore, this newly identified an Ezh2-p53 competition pattern may also play a role in modulating cancer biology in inflammasome-dependent or inflammasome-independent manners.

In conclusion, we identified a methylation-independent role of Ezh2 in mediating lncRNA *Neat1* transcription for inflammasome activation and related pathologies through the Ezh2-p53 competition pattern. In this process, Ezh2 functioned through its SANT2 domain to bind to the *Neat1* gene promoter to maintain H3K27ac enrichment and thus facilitate p65-mediated *Neat1* transcription, whereas p53 recruited SIRT1 to deacetylate H3K27, leading to suppression of *Neat1* transcription (Fig. 8). Targeting the Ezh2 SANT2 domain may have beneficial effects in inflammasome-related diseases.

MATERIALS AND METHODS

Mice

C57BL/6 background *Ezh2* flox mice and *Tp53* flox mice were as previously described [15, 51], and were crossed with lysozyme M-cre mice to produce myeloid cell-conditional knockout mice. The *Neat1*$^{-/-}$ mice were gifted by Prof. Mian Wu (University of Science and Technology of China, China) [8]. All mice were maintained in a specific pathogen-free facility, and all animal experiments were complied with all relevant ethical regulations for animal testing and research, and were in accordance with protocols approved by the institutional Biomedical Research Ethics Committee, Shanghai Institute of Nutrition and Health, Chinese Academy of Sciences.

Plasmids, antibodies and reagents

The Ezh2 expression plasmid were as previously described [15]. HA-Ezh2 and Ezh2 truncations were cloned from the cDNA encoding full-length Ezh2 into pcDNA-vector. The flag-Ezh2, flag-Ezh2ΔSANT2 and flag-Ezh2ΔSET were cloned into pLVX-GFP-vector. The expression plasmids for NLRP3, ASC and Caspase-1 were gifted by Prof. Shuo Yang (Nanjing Medical University, China), the expression plasmids for acetyltransferases (CBP, p300, PCAF, Tip60) and deacetylases (HDAC1-6, SIRT1-7) were as

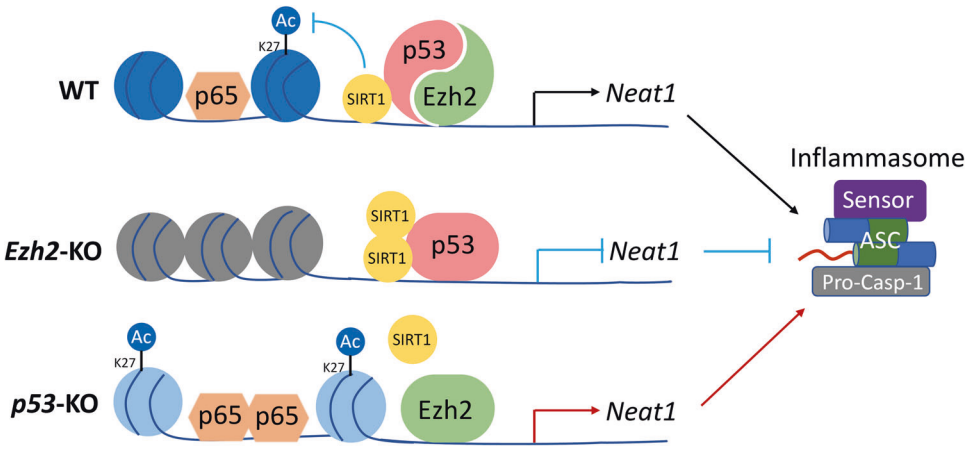

Fig. 8 The Ezh2-p53 competition modulates inflammasome activation. Upon stimulation with various inflammasome inducers in wild-type (WT) cells, Ezh2 excludes p53 to bind to the promoter of lncRNA *Neat1* gene, maintains the H3K27ac enrichment and chromatin accessibility, thereby facilitating p65-mediated *Neat1* transcription for inflammasome activation. *Ezh2* deletion increases the p53 binding to the *Neat1* gene promoter, and p53 recruits the deacetylase SIRT1 for H3K27 deacetylation, which suppresses p65 binding to the *Neat1* gene promoter for its transcription and thus inhibits inflammasome activation. In contrast, *p53* deficiency abolishes SIRT1 recruitment and thus enhances H3K27ac at *Neat1* gene promoter and then promotes p65-mediated *Neat1* transcription.

previous described [52], the expression plasmids for STAT1 and STAT3C were as previously described [53], and the expression plasmids for C/EBPα and C/EBPβ were as previously described [54]. *Neat1* promoter regions (−1.4k to +0.1k) were amplified by PCR from mouse genomic DNA and then inserted to PGL4.22 [luc2CP/Puro] vector (E677A, Promega). Neat1 overexpression plasmid was gifted by Prof. Mian Wu (University of Science and Technology of China, China) [8]. All sequences of homemade and requested constructs were confirmed by DNA sequencing.

The antibodies against Ezh2 (5246s), H3K27me3 (9733s), IL-1β (12242), SIRT1 (8469S), IgG (2729s) and p53 (2524S) were from Cell Signaling Technology. Antibodies for β-actin (A2228) and Flag (A8592) were from Sigma-Aldrich. Antibody for p65 (C-20, sc-372) was from Santa Cruz. Antibodies for Caspase-1 (AG-20B-0042), ASC (AG-25B-0006) and NLRP3 (AG-20b-9014) were from AdipoGen Life Sciences. Antibody for H3K27ac (ab4729) was from Abcam. Antibody for Iba1 (019-19742) was from WAKO. Antibody for GSDMD was from abcam (ab209845). Antibody for TH (MAB318) was from chemicon. Antibody for HA (2013819) was from Roche. LIVE/DEAD™ Fixable Violet Dead Cell Stain (L34964), FITC-mouse CD45 antibody (11-0451-85), APC cy7-mouse CD11b antibody (47-0112-82), Percp cy5.5-mouse Gr1 antibody (45-5931-80), PE-mouse F4/80 antibody (12-4801-82), Anti-Mouse IgG Alexa Fluor Plus 488 (A32723) and Anti-Rabbit IgG Alexa Fluor 594 (A21207) were from Thermo Fisher Scientific. Anti-Linear ubiquitin antibody was a gift from Dr. Vishva Dixit (Genentech, USA).

LPS (L3129), ATP (A2383) and 6-OHDA (h4381) were purchased from Sigma-Aldrich. MSU (tlrl-msu-25) and poly (dA:dT) (tlrl-patc) were from InvivoGen. Flagellin (AG-40B-0125) was from AdipoGen. DOTAP Liposomal Transfection Reagent (11202375001) was from Roche. Protein A/G magnetic beads (HY-K0202), Nigericin (HY-100381) and GSK126 (HY-13470) were from MedChemExpress. Vectastain ABC (PK4000) and IgG biotin (BA1000) were from vector lab. DZNeP (S7120), EED226 (S8496), EX527 (S1541), Nicotinamide Riboside Chloride (S2935), β-Nicotinamide Mononucleotide (S5259) and Nutlin3 (S1061) were from SelleckChem. Thioglycolate broth (211716) was from BD. SYBR qPCR SuperMix Plus (E096-01B) was from Novoprotein. Proteinase K (A300491), Anti-Fade Mounting Medium (E675011), BSA (A602440), puromycin (A610593) and DAPI (A606584) were from Sangon Biotech. FBS (10270), 2-mercaptoethanol (21985023), penicillin-streptomycin (15140-122), and GlutaMAX Supplement (35050-061) were from Gibco. DMEM/High Glucose (SH30243.01) and RPMI Medium Modified (SH30809.01) were from Hyclone. Protease inhibitor cocktail (B14001) and phosphatase inhibitor cocktail (B15001) were from Bimake. LipoFiterTM Liposomal Transfection Reagent (HB-LF10001) was from Hanbio. TRIzol reagent (15596018), RNase A (8003089), Lipofectamine RNAiMAX (13778075), Lipofectamine 3000 (L3000015) and Inject™ Alum Adjuvant (77161) were from Thermo Fisher Scientific. Dual-luciferase reporter assay system (E1960) was from Promega. The InVivoMAb anti-Mouse IL-1β (BE0246) was from BioXcell. The DNA library Prep Kit V2 for illumina (TD501-01) and Index Kit V2 for illumina (TD202) were from Vazyme.

Cell culture

Peritoneal macrophages were induced by intraperitoneally injection 4% thioglycolate broth (TB) into 6–8-week-old mice (2 ml/mouse). After 3–4 days, mice were euthanized, and the peritoneal cavity was flushed by 8–10 ml DMEM medium. Peritoneal exudate cells were collected and seeded with DMEM containing 10% FBS in the dish. Four hours later, removed unattached cells and macrophages were attached to the dish for the experiments.

Bone marrow derived macrophages (BMDMs) were cultured and induced by DMEM containing 20% FBS and L929 conditional medium. After 4 days culture, the adherent BMDMs could be digested by EDTA digest solution for further experiments.

Microglia were collected from the brains of newborn mice (24 h). Brain tissues were removed the meninges and digested with 0.25% trypsin at 37 °C, after 15–20 min filtered with a 70 μm mesh. The cells were then seeded with 10% FBS-DMEM/F12 medium in the dish. Twenty-four hours later, change the medium to remove unattached cells and then change new medium every 3 days until 21 days. Microglia were isolated through gentle digestion with 0.08% trypsin at 37 °C to removed astrocyte layer.

iBMDMs were cultured with DMEM medium containing 10% FBS, and were digested by EDTA digest solution for further experiments. THP-1 cells were cultured with RPMI 1640 medium containing 10% FBS, and were differentiated into macrophages by PMA (200 ng/ml) treatment for 24 h.

Induction of peritonitis

Sex-matched mice (8–10 weeks old) were intraperitoneal injected with 1 mg MSU (InvivoGen) or 700 μg Alum, and the control mice were injected with equal volume of PBS or TB (200 μl/mouse). Six hours later, peritoneal cavities were washed with 4 ml PBS, and the peritoneal exudate cells were collected for flow cytometry analysis. For IL-1β detection, the peritoneal fluids were concentrated by Amicon Ultra 10K (Millipore), and then IL-1β level was measured by ELISA. The WT or *Ezh2*-MKO mice were randomly allocated to different experimental groups.

6-OHDA model

Sex-matched mice (10 weeks old) were narcotised before unilateral intra-striatal perfusion of 1.8 μg 6-OHDA (in sterile 0.9% NaCl solution) or equal sterile 0.9% Nacl solution at ML, 1.8 mm; AP, −0.5 mm; DV, −3.5 mm. 3 days or 2 weeks after 6-OHDA treatment, mice were anaesthetised and perfused with 4% paraformaldehyde, then the brain tissues were fixed by 4% paraformaldehyde overnight, dehydrated by 30% sucrose (in PB solution) for 48 h and processed into frozen section for immunostaining.

Stimulation with inflammasome activators

The collected macrophages or microglia (about 1×10^6 cells/well in 12 wells plates) were starved with DMEM complemented with 0.5% FBS overnight, cells were primed with 200 ng/ml LPS for 4 h, and then stimulated with 10

μM nigericin (MCE), 2.5 mM ATP (Sigma) or Lipofectamine-transfected 1.6 μg/ml poly(dA:dT) (InvivoGen) for 1 h, or DOTAP-transfected 1 μg/ml flagellin (Adipogen) for 6 h.

Immunoblot, immunoprecipitation

For immunoblot analysis, cells were lysed with RIPA buffer containing protease inhibitors. For co-immunoprecipitation assays, the lysates from about 2×10^7 cells were incubated with the desired antibodies and the protein-A/G magnetic beads (MCE) overnight. And then the protein crossing beads were washed by RIPA buffer. Supernatant proteins were concentrated with equal methanol and a quarter of trichloromethane. The cell lysates, beads and supernatant protein were separated by SDS-PAGE and transferred onto nitrocellulose membrane (Millipore) for subsequently immunoblot. The full-length original western blots for these results are provided in Supplementary File 1.

ASC oligomerization assays and Phos-tag-based mobility shift assay (MSA)

About 1×10^6 cells were lysed with 0.5 %Triton X-100 in PBS containing protease inhibitor, 10% of the lysates were collected as whole-cell lysates and the rest were centrifuged at 7000 rpm for 15 min. The supernatant fractions were the Triton X-soluble, and the pellet fractions were the Triton X-insoluble. Those fractions were separated by electrophoresis through 10% polyacrylamide gels with or without 50 μM $MnCl_2$ and 25 μM phos-tag ligand (APExBIO). For ASC oligomerization analysis, the pellets were crosslinked for 30 min at room temperature with 2 mM disuccinimidyl suberate (Pierce) and then centrifuged for 15 min at 7000 rpm. The pellets were also separated by SDS-PAGE.

Reconstruction of the inflammasome system in HEK293 cells

HEK293T cells were cultured in 12-well plates before transfection, and then co-transfected with expression plasmids of pro-caspase-1, ASC and NLRP3 when the cell density reached 60–70%. The total amount of transfected plasmid DNA was adjusted to 1.6 μg/well with pcDNA3-empty-vector. The cells were cultured with 10% FBS-DMEM for at least 24 h, and then changed with 0.5% FBS-DMEM for further incubation for 12 h before inflammasome examination.

Immunofluorescent and immunohistochemical staining and analysis

For immunofluorescent staining, macrophages (about 2×10^5 cells/slice) or brain slices were fixed for 30 min with 4% cold paraformaldehyde at 4 °C and then permeabilized with 0.2% Triton X-100 in PBS for 5 min. Subsequently, cells were blocked with 3% BSA in PBS for 1 h, stained with specific primary antibodies and fluorescent-conjugated secondary antibodies. The nucleus was stained by DAPI. For immunohistochemical staining, brain slices were treated with 3% H_2O_2 for 30 min, and then blocked with 3% BSA in PBS for 1 h, successively stained with specific primary antibodies, biotin-conjugated secondary antibodies and avidin-conjugated third antibody (VECTOR). Finally, the slices were visualised by DAB Horseradish Peroxidase Color Development Kit (Beyotime). All the samples were photographed with ZEISS confocal microscopy and then quantified by using ImageJ as previously described [51, 55]. In brief, the integrated optical density (IOD) of NLRP3 was calculated by sampling a 403.23 × 403.23 μm area, in the striatum, in 8–10 fields taken from at least four sections. Values are presented as the sum of the optical density values of fluorescence intensity obtained from all the cells of each field. TH^+ neuron numbers were calculated by sampling a 2.02 × 2.02 mm area in the substantia nigra, in 4–8 fields taken from seven sections. ASC specks were measured by sampling a 108.70 × 108.70 μm area at least in three sections.

ELISA

The supernatants from the cell culture in 12 well plates (1×10^6 cells/well) and the peritoneal fluids were analysed for mouse IL-1β with Invitrogen ELISA kit. The protein standard was measured at the same plate. The optical density was analysed at OD_{405} and OD_{450} by Microplate Reader.

Luciferase reporter assay

The *Neat1* gene promoter-driven luciferase reporter plasmid was transfected with pRL-TK and other indicated expression vectors into HEK293Ts with LipoFiterTM Transfection Reagents. In some cases, siRNAs were transfected into HEK293T and followed by luciferase reporter plasmids transfection. The luciferase activity was measured by following the protocol of Dual-Luciferase Reporter Assay System, and the relative light units of chemiluminescence were measured with LB 9508 Lumat3 (Berthold Technologies).

Flow cytometry analysis

The peritoneal lavage fluids were collected in mice i.p. injected with MSU or Alum. After spun down at 1500 rpm for 5 min, the cells were incubated with the indicated antibodies for 30 min at 4 °C. Followed by washing with PBS, the cells were resuspended with PBS and analysed with Beckman Gallios machine.

Gene knockdown or knockout

Gene knockdown in macrophages and HEK293T cells were as previously described [56]. For the stable gene knockdown, the shRNA plasmids targeting *Neat1*, *p53* or *Sirt1* pLKO.1 vector were transfected into HEK293T cells along with lentiviral packaging vectors, psPAX2 and pMD2 for 48 h. Then the lentiviral supernatants were used to iBMDMs infection for 48 h. Next, puromycin (8 μg/ml) was added to select successfully infected iBMDMs. For the transient knockdown of *EZH2* and *P65* in HEK293T cells, the siRNAs purchased from GenePharma were transfected into cells using Lipofectamine RNAiMAX for at least 24 h. The knockdown efficiency was validated by immunoblotting or QPCR assays. The shRNA/siRNA sequences are shown in Supplementary Table 1.

For CRISPR-Cas9-mediated *Ezh2* deletion, the small guide RNA (sgRNA) sequence 5′-gaataatcatgggccagact-3′ were designed for targeting mouse Ezh2 at the web site (https://crispr.mit.edu/), which were then cloned into the LentiCRISPRv2 plasmid (Addgene). The plasmid was transfected into HEK293T cells along with lentiviral packaging vectors, psPAX2 and pMD2 for 48 h. The iBMDM were infected with lentivirus collected in the supernatants. After 48 h, iBMDMs were treated with puromycin (8 μg/mL) for selecting infected cells and the single cells were seeded into isolated wells of 96-well plates. After single clonal expansion, Ezh2 deletion efficiency was validated by sequencing and immunoblot analysis.

ChIP assay and ATAC-seq assay

Primary macrophages or iBMDMs (about 1×10^7 cells/sample) were fixed with 1% formaldehyde for 10–15 min at room temperature and quenched crossing-linking with 2.0 M glycine to a final concentration of 0.2 M for 10 min at room temperature. After rotating and washing, the cells were incubated with ice-cold ChIP lysis buffer to gain the nucleus. Next, the nucleus was sonicated to obtain the appropriate-length DNA fragment, then followed by immunoprecipitation with indicated antibodies. After protein degradation and washing with several buffers, the immunoprecipitated DNA was purified and subjected to high-throughput sequencing or QPCR analysis with different primers. All sequences of primers for ChIP-QPCR are shown in Supplementary Table 2.

For ATAC-seq, 5×10^4 viable primary macrophages were spun down at 500 RCF at 4 °C for 5 min in a fixed-angle centrifuge. Aspirate all supernatant, carefully avoiding visible cell pellet. And then add 50 μl cold ATAC-Resuspension Buffer (10 mM Tris-HCl pH 7.4, 10 mM NaCl, 3 mM MgCl2 and 0.1%NP-40) and pipette up and down 3 times. Incubate on ice for 3 min. Pellet nuclei at 500 RCF for 10 min at 4 °C in a fixed-angle centrifuge. Aspirate all supernatant, carefully avoiding visible cell pellet, then use Vazyme TD501 library prep kit for tagmentation. Subsequently, cleanup reaction with Qiagen QIAquick PCR Purification Kit and elute DNA in 24 μl sterile water. We used Vazyme TruePrepTM Index Kit V2 for Illumina for PCR amplification. Finally, purify libraries with 1.2× VAHTS DNA clean beads (Vazyme) for sequencing.

All of sequencing data were analysed by using the Galaxy Europe website (https://usegalaxy.eu) as follows. First, map the sequencing data with reference genome mm10, and then use MarkDuplicates to examine aligned records in BAM datasets to locate duplicate molecules. Second, use MACS2 for calling peaks from alignment result, and then convert bedgraph files into bigwig files for obtaining the normalised bigwig files. In addition, we used computeMatrix to prepare data for plotting a heatmap or a profile of given regions.

Electrophoretic mobility shift assay (EMSA)

Ten million primary macrophages were used to extract the nuclear protein. Nuclear extracts were prepared by using Nuclear and Cytoplasmic Protein Extraction Kit (Beyotime P0028) and then quantified through BCA protein assay (Pierce 23225). Electrophoretic mobility shift assay was performed by

using the EMSA/Gel-Shift Kit (Beyotime GS002) with a biotin-labelled probe (5′-gccacagagccaaaggagcccacgaggggcgggtcatgg-3′) based on mouse *Neat1* gene promoter. No less than 2 μg nuclear protein and 10 fmole probe were used in each test. In some experiments, 2 μl of anti-Flag antibody was added to the nuclear extract 10 min before the addition of labelled probe, antibody could bind with target protein and then abolished the migration of the protein-DNA probe complex into the EMSA membrane.

Mass spectrometry

To identify the potential binding protein of SIRT1, whole-cell lysates of HEK293T cells that transfected with Flag-SIRT1 were pre-cleaned with protein-A/G agarose beads, and then incubated with the Flag-conjugated M2 beads at 4 ℃ for overnight. Subsequently, the protein–beads complexes were washed by PBS and sent to process with cross-linking mass spectrometry analysis.

Real-time quantitative PCR

RNA was isolated by TRIzol reagent (TaKaRa) and reverse transcribed to cDNA by RT reagent Kit (TaKaRa). qRT-PCR was conducted with TB Green (TaKaRa) using a QuantStudio 7 Flex Real-Time PCR system (Applied Biosystems). The expression of individual genes was calculated by a standard curve method. Gene-specific PCR primers are listed in Supplementary Table 2.

Statistical analysis

The data are shown as mean ± SD, and unless otherwise indicated, all the presented data were the representative results of at least three independent repeats. Statistical analysis was performed by using GraphPad Prism (Graph-Pad Software), and the statistics were analysed by a two-tailed Student's *t* test or Multiple *t* test as indicated. Differences were considered to be significant at $p < 0.05$ and are indicated by *, those at $p < 0.01$ are indicated by **, and those at $p < 0.001$ are indicated by ***.

DATA AVAILABILITY

The RNA-Sequencing, ChIP-Sequencing and ATAC-Sequencing data have been deposited into the Gene Expression Omnibus (accession code GSE101383, GSE79423, GSE197086 and GSE181944). All other data supporting the findings of this study are available from the corresponding author on reasonable request.

REFERENCES

1. Mamik MK, Power C. Inflammasomes in neurological diseases: emerging pathogenic and therapeutic concepts. Brain. 2017;140:2273–85.
2. Martinon F, Pétrilli V, Mayor A, Tardivel A, Tschopp J. Gout-associated uric acid crystals activate the NALP3 inflammasome. Nature. 2006;440:237–41.
3. Man SM. Inflammasomes in the gastrointestinal tract: infection, cancer and gut microbiota homeostasis. Nat Rev Gastroenterol Hepatol. 2018;15:721–37.
4. Rathinam VA, Vanaja SK, Fitzgerald KA. Regulation of inflammasome signaling. Nat Immunol. 2012;13:333–42.
5. He Y, Hara H, Núñez G. Mechanism and regulation of NLRP3 inflammasome activation. Trends Biochem Sci. 2016;41:1012–21.
6. Dick MS, Sborgi L, Ruhl S, Hiller S, Broz P. ASC filament formation serves as a signal amplification mechanism for inflammasomes. Nat Commun. 2016;7:11929.
7. Hara H, Tsuchiya K, Kawamura I, Fang R, Hernandez-Cuellar E, Shen Y, et al. Phosphorylation of the adaptor ASC acts as a molecular switch that controls the formation of speck-like aggregates and inflammasome activity. Nat Immunol. 2013;14:1247–55.
8. Zhang P, Cao L, Zhou R, Yang X, Wu M. The lncRNA Neat1 promotes activation of inflammasomes in macrophages. Nat Commun. 2019;10:1495.
9. Cao R, Wang L, Wang H, Xia L, Erdjument-Bromage H, Tempst P, et al. Role of histone H3 lysine 27 methylation in Polycomb-group silencing. Science. 2002;298:1039–43.
10. Margueron R, Reinberg D. The Polycomb complex PRC2 and its mark in life. Nature. 2011;469:343–49.
11. Varambally S, Dhanasekaran SM, Zhou M, Barrette TR, Kumar-Sinha C, Sanda MG, et al. The polycomb group protein EZH2 is involved in progression of prostate cancer. Nature. 2002;419:624–29.
12. Reijm EA, Timmermans AM, Look MP, Meijer-van Gelder ME, Stobbe CK, van Deurzen CHM, et al. High protein expression of EZH2 is related to unfavorable outcome to tamoxifen in metastatic breast cancer. Ann Oncol. 2014;25:2185–90.
13. Eich ML, Athar M, Ferguson JE 3rd, Varambally S. EZH2-targeted therapies in cancer: hype or a reality. Cancer Res. 2020;80:5449–58.
14. Yap TA, Winter JN, Giulino-Roth L, Longley J, Lopez J, Michot JM, et al. Phase I study of the novel enhancer of zeste homolog 2 (EZH2) inhibitor GSK2816126 in patients with advanced hematologic and solid tumors. Clin Cancer Res. 2019;25:7331–39.
15. Zhang X, Wang Y, Yuan J, Li N, Pei S, Xu J, et al. Macrophage/microglial Ezh2 facilitates autoimmune inflammation through inhibition of Socs3. J Exp Med. 2018;215:1365–82.
16. Gunawan M, Venkatesan N, Loh JT, Wong JF, Berger H, Neo WH, et al. The methyltransferase Ezh2 controls cell adhesion and migration through direct methylation of the extranuclear regulatory protein talin. Nat Immunol. 2015;16:505–16.
17. Man SM, Kanneganti TD. Regulation of inflammasome activation. Immunol Rev. 2015;265:6–21.
18. Hornung V, Bauernfeind F, Halle A, Samstad EO, Kono H, Rock KL, et al. Silica crystals and aluminum salts activate the NALP3 inflammasome through phagosomal destabilization. Nat Immunol. 2008;9:847–56.
19. Gordon R, Albornoz EA, Christie DC, Langley MR, Kumar V, Mantovani S, et al. Inflammasome inhibition prevents α-synuclein pathology and dopaminergic neurodegeneration in mice. Sci Transl Med. 2018;10:eaah4066.
20. Boyer LA, Latek RR, Peterson CL. The SANT domain: a unique histone-tail-binding module? Nat Rev Mol Cell Biol. 2004;5:158–63.
21. Campagno KE, Mitchell CH. The P2X(7) receptor in microglial cells modulates the endolysosomal axis, autophagy, and phagocytosis. Front Cell Neurosci. 2021;15:645244.
22. Kim J, Lee Y, Lu X, Song B, Fong KW, Cao Q, et al. Polycomb- and methylation-independent roles of EZH2 as a transcription activator. Cell Rep. 2018;25:2808–20.e4.
23. Grunstein M. Histone acetylation in chromatin structure and transcription. Nature. 1997;389:349–52.
24. Gräff J, Tsai LH. Histone acetylation: molecular mnemonics on the chromatin. Nat Rev Neurosci. 2013;14:97–111.
25. Li P, Spann NJ, Kaikkonen MU, Lu M, Oh DY, Fox JN, et al. NCoR repression of LXRs restricts macrophage biosynthesis of insulin-sensitizing omega 3 fatty acids. Cell. 2013;155:200–14.
26. Crotti A, Benner C, Kerman BE, Gosselin D, Lagier-Tourenne C, Zuccato C, et al. Mutant Huntingtin promotes autonomous microglia activation via myeloid lineage-determining factors. Nat Neurosci. 2014;17:513–21.
27. Siersbæk R, Rabiee A, Nielsen R, Sidoli S, Traynor S, Loft A, et al. Transcription factor cooperativity in early adipogenic hotspots and super-enhancers. Cell Rep. 2014;7:1443–55.
28. Oishi Y, Spann NJ, Link VM, Muse ED, Strid T, Edillor C, et al. SREBP1 contributes to resolution of pro-inflammatory TLR4 signaling by reprogramming fatty acid metabolism. Cell Metab. 2017;25:412–27.
29. Adriaens C, Standaert L, Barra J, Latil M, Verfaillie A, Kalev P, et al. p53 induces formation of NEAT1 lncRNA-containing paraspeckles that modulate replication stress response and chemosensitivity. Nat Med. 2016;22:861–8.
30. Mello SS, Sinow C, Raj N, Mazur PK, Bieging-Rolett K, Broz DK, et al. Neat1 is a p53-inducible lincRNA essential for transformation suppression. Genes Dev. 2017;31:1095–108.
31. Nakamura K, Zhang M, Kageyama S, Ke B, Fujii T, Sosa RA, et al. Macrophage heme oxygenase-1-SIRT1-p53 axis regulates sterile inflammation in liver ischemia-reperfusion injury. J Hepatol. 2017;67:1232–42.
32. Sugimoto K, Toyoshima H, Sakai R, Miyagawa K, Hagiwara K, Ishikawa F, et al. Frequent mutations in the p53 gene in human myeloid leukemia cell lines. Blood. 1992;79:2378–83.
33. Black JC, Van Rechem C, Whetstine JR. Histone lysine methylation dynamics: establishment, regulation, and biological impact. Mol Cell. 2012;48:491–507.
34. Li P, Ge J, Li H. Lysine acetyltransferases and lysine deacetylases as targets for cardiovascular disease. Nat Rev Cardiol. 2020;17:96–115.
35. Tan JZ, Yan Y, Wang XX, Jiang Y, Xu HE. EZH2: biology, disease, and structure-based drug discovery. Acta Pharm Sin. 2014;35:161–74.
36. Xu K, Wu ZJ, Groner AC, He HH, Cai C, Lis RT, et al. EZH2 oncogenic activity in castration-resistant prostate cancer cells is Polycomb-independent. Science. 2012;338:1465–9.
37. Lv Q, Xing Y, Liu J, Dong D, Liu Y, Qiao H, et al. Lonicerin targets EZH2 to alleviate ulcerative colitis by autophagy-mediated NLRP3 inflammasome inactivation. Acta Pharm Sin B. 2021;11:2880–99.
38. Rohraff DM, He Y, Farkash EA, Schonfeld M, Tsou PS, Sawalha AH. Inhibition of EZH2 ameliorates lupus-like disease in MRL/lpr mice. Arthritis Rheumatol. 2019;71:1681–90.
39. Zhang F, Wu L, Qian J, Qu B, Xia S, La T, et al. Identification of the long noncoding RNA NEAT1 as a novel inflammatory regulator acting through MAPK pathway in human lupus. J Autoimmun. 2016;75:96–104.
40. Wang Y, Hou L, Yuan X, Xu N, Zhao S, Yang L, et al. LncRNA NEAT1 targets fibroblast-like synoviocytes in rheumatoid arthritis via the miR-410-3p/YY1 axis. Front Immunol. 2020;11:1975.

41. Wang S, Zuo H, Jin J, Lv W, Xu Z, Fan Y, et al. Long noncoding RNA Neat1 modulates myogenesis by recruiting Ezh2. Cell Death Dis. 2019;10:505.
42. Huang S, Wang Z, Zhou J, Huang J, Zhou L, Luo J, et al. EZH2 inhibitor GSK126 suppresses antitumor immunity by driving production of myeloid-derived suppressor cells. Cancer Res. 2019;79:2009–20.
43. Zhou J, Nie D, Li J, Du X, Lu Y, Li Y, et al. PTEN is fundamental for elimination of leukemia stem cells mediated by GSK126 targeting EZH2 in chronic myelogenous leukemia. Clin Cancer Res. 2018;24:145–57.
44. Aasland R, Stewart AF, Gibson T. The SANT domain: a putative DNA-binding domain in the SWI-SNF and ADA complexes, the transcriptional co-repressor N-CoR and TFIIIB. Trends Biochem Sci. 1996;21:87–8.
45. Boyer LA, Langer MR, Crowley KA, Tan S, Denu JM, Peterson CL. Essential role for the SANT domain in the functioning of multiple chromatin remodeling enzymes. Mol Cell. 2002;10:935–42.
46. Guan X, Shi A, Zou Y, Sun M, Zhan Y, Dong Y, et al. EZH2-mediated microRNA-375 upregulation promotes progression of breast cancer via the inhibition of FOXO1 and the p53 signaling pathway. Front Genet. 2021;12:633756.
47. He XY, Xiang C, Zhang CX, Xie YY, Chen L, Zhang GX, et al. p53 in the myeloid lineage modulates an inflammatory microenvironment limiting initiation and invasion of intestinal tumors. Cell Rep. 2015;13:888–97.
48. Zhou CB, Fang JY. The role of pyroptosis in gastrointestinal cancer and immune responses to intestinal microbial infection. Biochim Biophys Acta Rev Cancer. 2019;1872:1–10.
49. Fang Y, Tian S, Pan Y, Li W, Wang Q, Tang Y, et al. Pyroptosis: a new frontier in cancer. Biomed Pharmacother. 2020;121:109595.
50. Zhang Z, Zhang Y, Xia S, Kong Q, Li S, Liu X, et al. Gasdermin E suppresses tumour growth by activating anti-tumour immunity. Nature. 2020;579:415–20.
51. Wang Y, Fu Z, Li X, Liang Y, Pei S, Hao S, et al. Cytoplasmic DNA sensing by KU complex in aged CD4(+) T cell potentiates T cell activation and aging-related autoimmune inflammation. Immunity. 2021;54:632–47.e9.
52. Yu T, Gan S, Zhu Q, Dai D, Li N, Wang H, et al. Modulation of M2 macrophage polarization by the crosstalk between Stat6 and Trim24. Nat Commun. 2019;10:4353.
53. Xiao Y, Zou Q, Xie X, Liu T, Li HS, Jie Z, et al. The kinase TBK1 functions in dendritic cells to regulate T cell homeostasis, autoimmunity, and antitumor immunity. J Exp Med. 2017;214:1493–507.
54. Xu J, Yu T, Pietronigro EC, Yuan J, Arioli J, Pei Y, et al. Peli1 impairs microglial Aβ phagocytosis through promoting C/EBPβ degradation. PLoS Biol. 2020;18:e3000837.
55. Shao W, Zhang SZ, Tang M, Zhang XH, Zhou Z, Yin YQ, et al. Suppression of neuroinflammation by astrocytic dopamine D2 receptors via αB-crystallin. Nature. 2013;494:90–4.
56. Zhu Q, Yu T, Gan S, Wang Y, Pei Y, Zhao Q, et al. TRIM24 facilitates antiviral immunity through mediating K63-linked TRAF3 ubiquitination. J Exp Med. 2020;217:e20192083.

ACKNOWLEDGEMENTS

We thank Drs. Mian Wu and Pengfei Zhang (University of Science and Technology of China, China) for the generous gift of *Neat1*-KO mice and *Neat1* expression plasmid, and Dr. Jiawei Zhou (Chinese Academy of Sciences, China) for the assistance to generate 6-OHDA-induced PD-like mouse model.

AUTHOR CONTRIBUTIONS

JY and QZ designed and performed the experiments, prepared the figures, and wrote part of the manuscript; XZ, ZW, GZ, YP, YW, SP and JX contributed to the experiments; NL and JQ contributed to ChIP-seq data analysis; PJ and WL contributed to *p65*-knockdown Raw2647 cells; CP contributed to mass spectrum analysis; QC supervised a specific subset of the experiments and analyses; YX initiated, designed and supervised this study, prepared the figures and wrote the manuscript. All authors read and approved the final paper.

FUNDING

This research was supported by grants from the National Natural Science Foundation of China (82030041, 82001657), the Strategic Priority Research Program of the Chinese Academy of Sciences (XDB39030300), the National Key R&D Program of China (2018YFA0107201, 2018YFA0902703), the programmes from Shanghai Municipal Science and Technology (20XD1424600, 21140905000), China Postdoctoral Science Foundation (2021M702163, 2021M700160, 2021M693272), Special Research Assistant Funding Project of the Chinese Academy of Sciences (QZ), Shanghai Post-doctoral Excellence Program (2021438 for QZ) and CAS Key Laboratory of Tissue Microenvironment and Tumor.

COMPETING INTERESTS

The authors declare no competing interests.

ETHICS STATEMENT

Our studies did not include human participants or human tissue. For the animal studies, experiments were performed according to the protocols approved by the institutional Biomedical Research Ethics Committee, Shanghai Institute of Nutrition and Health, Chinese Academy of Sciences.

ADDITIONAL INFORMATION

Supplementary information The online version contains supplementary material available at https://doi.org/10.1038/s41418-022-00992-3.

Correspondence and requests for materials should be addressed to Qian Cao or Yichuan Xiao.